Reply to Referee #1

Adam Majewski[1], Jeffrey R. French[1]

[1]Department of Atmospheric Science, University of Wyoming, Laramie, 82070, USA

Correspondence to: Adam Majewski (amajewsk@uwyo.edu)

We thank the reviewer for pushing us to better quantify the link between SCVVFs and SCDDs and pointing out a number of clerical errors. This, together with comments from the other reviewer led to a significant revision of the manuscript. We believe that the revised manuscript is easier to read, more consistent throughout, and provides conjecture and explanations that are better supported by the observations presented.

Below, comments provided by the reviewer are in black, our responses are in red.

Reviewer Comments

The paper uses in-situ observations of dynamics and microphysics to link the formation of supercooled drizzle drops to specific dynamical conditions.
Main comment: While the in depth interpretation of the flight leg data and back of the envelope discussion calculations were interesting, to me it seems that this qualitative investigation of this flight is the first part of the study**. The hypothesis proposed is that scvvf are required to form scdd**. I think it would be useful and necessary to generate some quantification of the observations to test this hypothesis using the rest of the flight data available from the campaign.

The bolded statement above mis-represents the intent of this manuscript. Through this work we aim to demonstrate that the presence of SCVVFs *enhance* drizzle formation and growth and therefore can influence where drizzle may form within clouds. This by itself is not surprising or novel. Throughout the introduction we present several previous studies linking the production of drizzle, in both supercooled clouds and in warm clouds, to atmospheric phenomena such as wind shear, turbulent mixing, cloud top instabilities, etc., which act to broaden the DSD. Further restrictions may be placed on *SCDD* development such as low CCN to grow larger droplets and INP concentrations to inhibit ice growth. The previous works focus on drizzle production predominantly at *cloud top.* Here we demonstrate that SCVVF layers can lead to drizzle initiation in the middle of a cloud, and need not occur at cloud top if the conditions are right. The observations presented from this case coupled with the concepts derived from earlier studies set up our hypotheses and eventual conclusions: that SCVVFs (1) can enhance collision-coalescence growth in a macroscopic sense (inferred from vertical reflectivity gradients), (2) can influence the vertical location of collision-coalescence onset in cloud (first occurring where SCVVFs are present), and (3) fundamentally affect the cloud microphysical response by condensation (subadiabatic w'-CWC' relationship). It is not our intent to suggest that SCVVFs are a necessary condition for SCDD production. In fact, we present observations from leg 2 showing the presence of drizzle despite the *absence* of SCVVFs. This is similarly true near the far eastern end of leg 1, where drizzle is present without SCVVFs. In these cases, drizzle initiation is presumably occurring near cloud top. Care has been taken in the revised manuscript to make this point more clear to the reader.

Based on the qualitative hypothesis it would seem reasonable to try and define thresholds for the following conditions: 1. T<0 and T>Tmin 2. ice_conc < min_ice_conc 3. are scvvf present? Need some metric based on w' ? 4. are scdd present? Need some metric based on cloud probes. and then combine these to quantify how well the scvvf-scdd hypothesis works. 1 and 2 have previously been suggested as controlling factors (as pointed out in the paper), while 3 is the new part explored here. So, if(1 & 2 & 3) is true, is 4 also true? This can be assessed for different thresholds and metrics across the flight campaign. Such an approach could also be used to assess the frequency and usefulness of the S anticorrelation seen to be indicative of scdd. I think this level of quantification would be very useful for other researchers and have application in aviation safety.

While we agree with the reviewer that such a study would be very interesting and useful, it is completely separate from the work presented here. The case-study approach used here aims to provide insight into the mechanisms important for influencing SCDD formation and growth. One expects that this in turn can be used to inform and validate future detailed modeling studies that aim to reproduce SCDD development in case clouds. A subsequent, campaign-wide examination of the role of SCVVFs in hydrometeor growth should help inform us regarding their overall role in SCDD formation in general, but provides little insight into the mechanism(s) responsible.

Specific Comments

l46 - S* and CCN not defined
The symbol S* is removed in the revised manuscript. CCN now defined in paragraph 3 in the Introduction: "(i.e. with lower numbers of cloud condensation nuclei; CCN)"
Care has been taken throughout the revised manuscript to ensure all symbols and abbreviations are defined.

l55 - and riming....
Riming has been included in the revised manuscript. We also note the following sentence captures this by stating: "....else ice will more rapidly scavenge the available vapor and cloud water." Paragraph 4 of Introduction in revised manuscript.

l68 - what mechanism? Is it shear induced turbulent enhancement?
Changed to explicitly indicate "turbulent broadening or mixing". Middle of paragraph 5 of the Introduction in revised manuscript

l85 - what gradient? Number concentration with temperature or horizontal distance?
This entire paragraph has been removed in the revised manuscript.

l151 - could report the frequency (Hz) of the data here for the size distributions, concentrations and condensed water estimates.
Change made, revised manuscript now reads: "From these 1 Hz size spectra…" in describing the size distributions and derived water content estimates. Paragraph 5, Section 2 of the revised manuscript.

L212: confirmed by the 2dp - was shape recognition used for the 2dp, or was the 99th percentile based on a size threshold?
The resolution (200 µm) of the 2DP is too coarse for reliable shape recognition. Rather, 2DP measurements were only used for particles with diameters greater than 1 mm (Paragraph 5, Section 2). Visual inspection of 2DS images failed to reveal any obvious liquid drops, *i.e. very circular particles,* with diameters larger than about 500 µm. Therefore, we presume that any particles larger than 1 mm, detected by the 2DP are likely ice. Regardless of whether these particles are liquid or ice, it does not change the conclusion that the concentration of ice particles was less than 0.1 L^{-1} in legs 1 and 2 and 0.3 L^{-1} in leg 5.

L218: "suggesting ice" - can liquid be ruled out? The doppler velocity would seem to be a potential evidence stream, but the text following this line seems to suggest it would be ambiguous.
We thank the reviewer for pointing this out. We often observed a significant decrease in Doppler velocity within about 1 km of the surface (Fig. 4e and 4f, for example, 20 to 40 km downwind of PJ). This decrease occurs at a similar location to a corresponding increase in the radar reflectivity, further bolstering the conjecture that liquid is being transformed to ice and that subsequent growth leads to enhanced reflectivity near the surface. This has been included in the revised manuscript. Paragraph 2 of Section 3.2.

L232: it seems that the plots and analysis could be passed through a high-pass filter to remove the terrain induced larger scale fluctuations and just concentrate on the smaller scale variations.
l271 - okay fig5b has w', but it is not clear what the nature of the filtering was of w to derive w'.
In order to calculate perturbation vertical velocity (i.e. *w'*), we took the measured vertical velocity and subtracted a simple high-pass filtered field that had been processed with a 10-s boxcar moving average. Several different size filters were tried, and the 10-s filter seemed to adequately capture the perturbations of interest. The details of this calculation are now included in the caption of Fig. 5 in the revised manuscript.

L274: to me the correlation between Ncld and w' looks poor - can you plot scatter plots and give correlation coefficients - or even do lagged correlations given the discussion at the end of the paper? fig5d shows the mvd and Ncld to have an almost linear anticorrelation, suggesting that Ncld is proportional to LWC^(-0.5). I don't know if that is a coincidence or if it means something significant...
Both reviewers commented on the correlations between droplet number concentration/liquid water content and perturbation vertical velocity. This also plays into the development of the conceptual model, presented as figure 13 in the manuscript. In order to address both reviewers, we provide additional analysis showing computed lagged correlations and follow-on discussion at the end of each review response (see below).

To the reviewer's other comment--there is clearly a strong anticorrelation between cloud droplet number concentration and mean-volume diameter, although what is not clear from the figure is whether it is linear. In the case of a linear (or near linear) relationship, we wonder if this demonstrates a balance between growth through condensation, collision-coalescence, and removal of drops through scavenging/collection and sedimentation. Exploring this in future work, particularly using detailed parcel model frameworks may be worthwhile.

l332 - the hypothesis was posed earlier on that the SCVVFs were responsible for the SCDD, but now this observation seems to counter that. See my main comment above.

We point out again, that the hypothesis is that SCVVFs may *enhance* drizzle production, but are not *required* (or responsible) for the initiation of SCDDs. However, in the example referenced here (leg 5), SCVVFs are indeed present and SCDDs are sampled at flight level. The principal difference in leg 5 compared to leg 1 is just that the SCVVF's are contained within a thin layer just above flight level. The SCVVFs in leg 5 are described in the second-to-last paragraph in section 3.4

L351: can you quantify this S correlation pattern to use it automatically?
That is an interesting question...given the observations from this single case study, it would not be possible to derive a quantification to be applied automatically. However, it may be worth exploring in a broader study that uses many cases (across the entire SNOWIE campaign, for instance) to look for a robust signal. Such an effort is beyond the scope of this study, but could be folded into a subsequent campaign-wide examination of SCVVFs as noted in an earlier response.

l373 Ncdp is this the same as Ncld?
All reference to Ncld and Ncdp has been removed from the text and replaced with the more explicit "cloud droplet number concentration" in the revised manuscript.

L407: is it possible to show a figure like 13 but from the actual data? I find it difficult to identify this behaviour in the current figures. It's difficult to see, but do the doppler velocity and reflectivity fields also show this lag effect?
Based on the results of the lagged correlations (below) this figure has been significantly revised. We acknowledge that the original figure was difficult to interpret and the connections between the ideas represented in the figure and the observations were not well represented. The revised figure is much simpler, and these connections are more apparent. We also note that the observed behavior supporting this model is best seen in the flight level data because of the noted complexity of the Doppler velocity data.

Condensational Inertia and Conceptual Model

R1: To me the correlation between Ncld and w' looks poor - can you plot scatter plots and give correlation coefficients - or even do lagged correlations given the discussion at the end of the paper?
R2: The schematic diagram presented in Fig. 13 is interesting, but I believe that the condensational inertia theory of why the LWC and Nd estimates are not in quadrature is insufficient. As the authors argue, the condensational delay may be around 10 seconds (phase relaxation timescale), yet the time between wave crests is substantially longer than this (probably 100 s or more for wind speeds of 10-20 m/s and wavelengths of 1-2 km).
Both referees indicated a desire for better quantification of the relationship between w' and CWC'/N_{cld}'. For referee 1 this had to do with some suggested N_{cld}/CWC relationship while for referee 2 it concerned the time/spatial scales and the lack of time series signals being in the expected quadrature relationship as per the proposed conceptual model (Fig. 13). To examine these relationships more quantitatively, the higher (5 Hz) resolution w', CWC', and N_{cld}' time series for were detrended and filtered of frequencies smaller than 0.1 Hz (wavelengths longer than 1 km). These time series were lagged by 0.2 s increments over a full 10 s period and correlated with a Pearson autocorrelation function to determine the correlation coefficients at each time lag. The results are presented below:

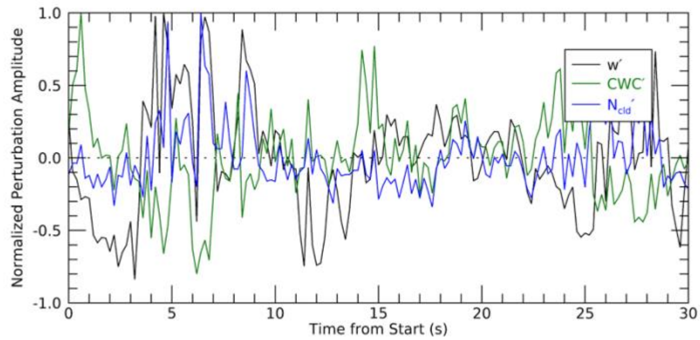

Figure 1: Normalized perturbation time series for selected kinematic and microphysical measurements. Measurements have been de-trended and filtered of frequencies lower than 0.1 Hz (corresponding to wavelengths longer than ~1 km).

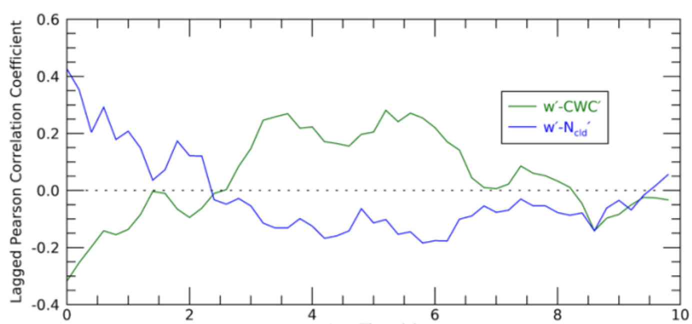

Figure 2: Lagged Pearson correlation coefficients for the time perturbation quantities in Fig. 1.

The lagged correlations (with maxima at position 0) clearly indicate that these condensational kinetic responses are zero-lag, with w'-CWC' being anticorrelated and w'-N_{cld}' positively correlated. Zero-lag correlations in this context likely indicate that cloud parcels are moving with(in) the kinematic pattern as opposed to through it as the latter should result in some spatial lag corresponding to the motion of parcels relative to w' pattern. This analysis has led us to modify the conceptual model presented in the original conceptual model with a more simple one. The analysis, while discrediting the original model, otherwise strengthens the suggested microphysical response. Furthermore, for the phase relaxation time to have led to a spatial lag exactly in quadrature now seems obviously unlikely, and we thank the referees for asking us to quantify these relationships. A new conceptual model incorporating this insight is proposed with perturbations caused from kinetic responses to a vertical velocity couplet more closely resembling the overturning cells suggested in HM05 to avoid the flow continuity issues that arise from this vertical parcel motion framework (e.g. when considering the location of maximum vertical displacement of parcels).

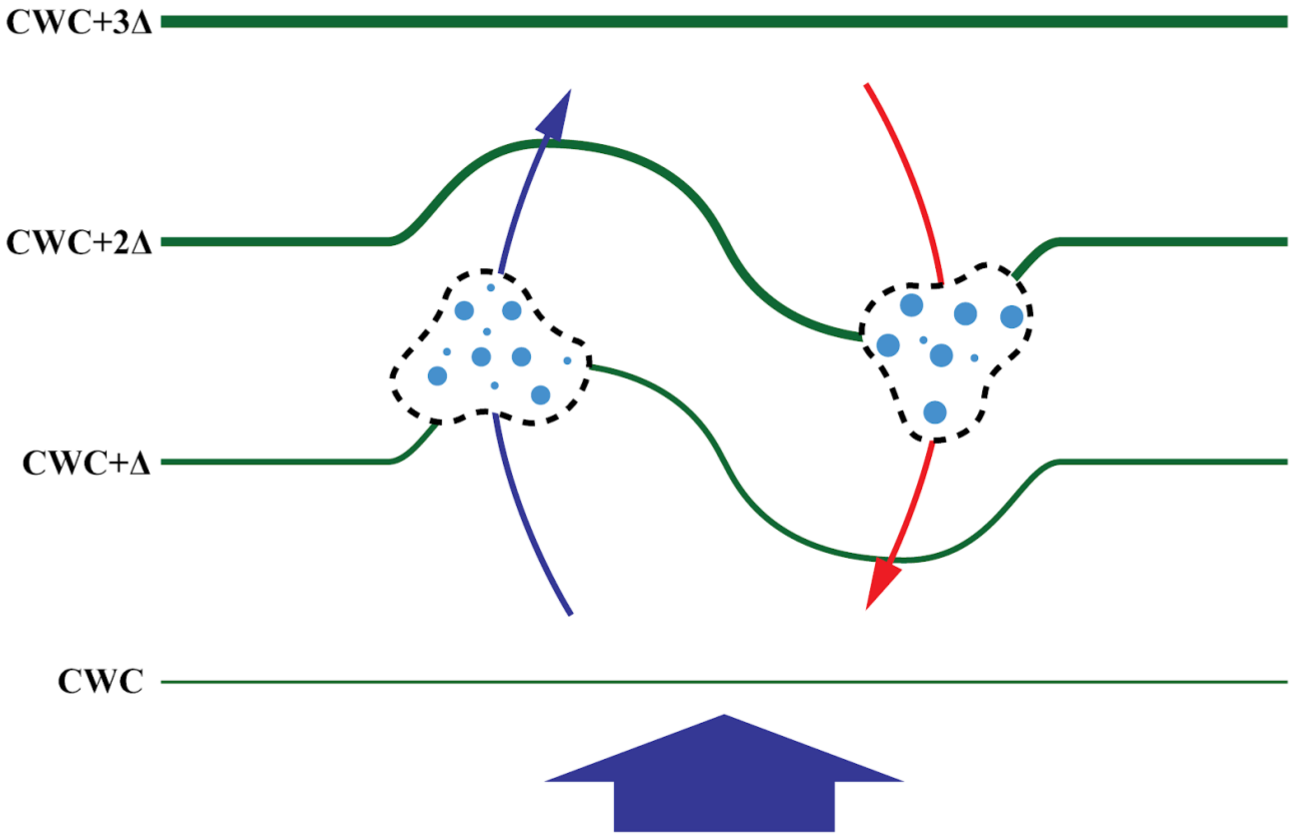

Figure 3: Revised conceptual model: simplified schematic of spatial responses to the perturbation updraft (blue) and downdraft (red) pattern superimposed on broader orographic lift (broad blue arrow bottom). The colored trajectories indicate the approximate path of parcels passing through the kinematic pattern following the schema of Houze and Medina (2005). Lines of constant cloud water content (green) indicating the expected deformations due to condensational kinetic effects, with line weight corresponding to relative condensate mass. Cloud parcels circulate within the vertical velocity perturbation pattern and more and smaller drops are located in perturbation updrafts than downdrafts. CWC contours appear flat and unperturbed above and below the vertical velocity fluctuation pattern as they are determined by the adiabatic ascent in the broader uplift pattern.

References

Houze, R. A. and S. Medina, : Turbulence as a Mechanism for Orographic Precipitation Enhancement, J.Atmos.Sci., 62, 3599-3599-3623, https://doi.org/10.1175/JAS3555.1, 2005.

Reply to Referee #2

Adam Majewski[1], Jeffrey R. French[1]

[1]Department of Atmospheric Science, University of Wyoming, Laramie, 82070, USA

Correspondence to: Adam Majewski (amajewsk@uwyo.edu)

We thank the reviewer for pushing to broaden the applicability and better articulate the novelty of the results and also for challenging us to better quantify the perturbation correlations, leading to a change to the conceptual model that seems to agree better with the flight data. This, together with comments from the other reviewer led to a significant revision of the manuscript. We believe that the revised manuscript is easier to read, more consistent throughout, and provides conjecture and explanations that are better supported by the observations presented.

Below, comments provided by the reviewer are in black, our responses are in red.

Reviewer Comments

This paper explores aircraft observations using a W-band radar and in-situ measurements of state parameters, wind motions, and cloud and drizzle drop size distributions within a supercooled layer cloud flowing over heterogeneous terrain. The authors find correlations between km-scale somewhat vertically coherent fluctuations in vertical motion and microphysical changes in the cloud. The measurements appear to support the idea that small scale fluctuations in such clouds may be sufficient to push an otherwise non-drizzling cloud into a state whereby it produces precipitation.
I found the manuscript to be adequately well-written, although the authors should pay better attention to spelling (Rosemount is mis-spelled in several occasions), grammar, and precision in their scientific writing.
Comments from both reviewers have led to a significant revision of the manuscript. In this revision, we have taken care to be more consistent with our wording, grammatically correct and consistent, and more precise in our descriptions. Because of this, we believe that the revised manuscript is easier to read and contains fewer inconsistencies that can lead to reader mis-understanding.

The results, while interesting, are not particularly novel (see e.g. Houze and Medina 2005, who have already documented such correlations between small-scale vertical motions and radar-derived microphysical properties). It is a little unclear how the results presented would move our knowledge base forward.
Houze and Medina (2005; HM05 for brevity) examined the enhancement of precipitation by turbulent overturning cells in coastal frontal systems with contained a significant orographic forcing. At relatively large spatial scales (broad udrafts and large swaths of available condensate) and small spatial scales (~kilometer scale vertical motions embedded in layers of shear-driven overturning cells) orography was shown to modify the flow field to generate or otherwise enhance condensate supply rates, increasing upstream precipitation via increased collectional growth where condensate was locally concentrated. Although the cases analyzed were principally of precipitating mixed phase clouds with active ice nucleation processes, the authors suggested that for clouds with the 0 °C isotherm nearer the surface or with embedded bright bands, these turbulent overturning cells would be expected to similarly enhance growth rates for falling liquid hydrometeors. It is precisely in this context that several of our findings here are novel: (1) despite the w-LWC relationship reported in HM05 for mixed phase clouds (+w' and +LWC' on average), we found the opposite correlation which we believe to be a function of low droplet number concentration; (2) collectional growth still appeared to be enhanced through these layers despite the inverse w'-LWC' relationship; and (3) vertical location of initial collision-coalescence activity appeared to be tied to these layers even well below cloud top. For these reasons, this not only serves as a strong addendum to HM05 with respect to liquid or mostly

liquid clouds, but also raises questions as to whether turbulent motions, locally enhanced SLW pockets, or something else (e.g. condensational kinetic effects for liquid, lengthened trajectories for ice, etc) are responsible for the faster hydrometeor growth noted in these layers *for all conditions*.

The authors need to work harder to make their results appealing to the broader cloud physics community.
Care has been taken in the revised manuscript to place these results in the context of all highly supercooled liquid clouds (for instance, paragraph 7, Section 1; and paragraph 1, Section 5), liquid clouds with marine aerosol character (paragraph 5, Section 1), and to simplify the conceptual model as much as possible (paragraph 3, Section 4.1).

The schematic diagram presented in Fig. 13 is interesting, but I believe that the condensational inertia theory of why the LWC and Nd estimates are not in quadrature is insufficient. As the authors argue, the condensational delay may be around 10 seconds (phase relaxation timescale), yet the time between wave crests is substantially longer than this (probably 100 s or more for wind speeds of 10-20 m/s and wavelengths of 1-2 km). More quantification of this would be helpful.
Comments from both reviewers has led to additional analysis investigating correlations of perturbation quantities. This has resulted in a significant revision to the schematic diagram (Fig. 13) in the revised manuscript. Details of this are provided at the end of our comments.

Why isn't the removal of droplets by coalescence also playing a key role?
This is explicitly addressed in paragraph 4, Section 4.1: The remaining magnitude of CWC variation is likely related to the precipitation dynamics. Removal of cloud water by scavenging from drizzle in perturbation updrafts would lead to lower CWC's and reduced cloud droplet number."

Why is there no map showing the synoptic conditions, horizontal flow pattern etc?
We included no map of the synoptic conditions because we felt they were adequately described in the exposition of the case context, and that the bulk thermodynamic conditions were more enlightening in describing how and where clouds formed. Here we try to strike a balance between completeness and length of manuscript. Synoptic maps can be found in the Master's Thesis from which this manuscript was developed (Majewski 2019; Fig. 3.1, p. 55).

Where are the Payette mountains?
The Payette mountains are a locally-used reference to the western-most foothills of the broader Sawtooth Range. In the revised manuscript all reference to the Payette mountains has been removed and reference is now made to the Sawtooth Range, consistent with the map shown in Fig. 1.

I think the data here could be analyzed in a much more quantitative manner than is presented here. What is the vertical coherence of the small-scale vertical motions as seen by the WCR? This is why we have radars. Yet the radar here is underutilized.
Some attempt to quantify the coherence of the Doppler velocities and the reflectivities have been done in a statistical sense for the CFAD columns with the vertical profile of bulk correlation coefficients. However, going beyond this to investigate the coherence of small-scale motions is not trivial, given the convolved nature of what is measured by the Doppler radar. Variations in hydrometeor terminal fall speeds, especially for drizzle, are much larger than variations in vertical air motion.

Fig. 7 states that hydrometeor Doppler motions are shown, but this implies that the vertical wind field is known. How can this be? This needs some correction to explain what is shown and what was done to remove the wind motions.
Figure 7a shows the measured *Doppler velocity*, as indicated in the caption (note this is the same as shown in Figs. 4, 10b, and 11b). No attempt has been made to de-convolve the vertical air motion from the hydrometeor terminal fall speeds in any of these images. This is explicitly stated in the revised manuscript, at the end of paragraph 3, Section 2 and again in paragraph 3, Section 3.2.

Note that in Figure 7b, we *estimate* the hydrometeor terminal fall speed for range gates located near the aircraft (both above and below flight level). This is done by subtracting the aircraft measured vertical air velocity from the radar measured Doppler velocity in these range gates. The description of this is found near the end of paragraph 3, Section 3.4.

It is interesting that the clouds are ultra clean (very low cloud droplet concentrations). Yet this is barely mentioned later. Is there a real bottleneck for drizzle production given this? The authors could quantify the coalescence by running an SCE solver on their size distributions to quantify the degree to which the clouds could produce drizzle without vertical motion enhancing LWC.
We agree. The very low droplet concentrations encountered on this day and throughout the field campaign were a very interesting (and surprising!) observation. We reference low droplet concentrations throughout the manuscript as we describe the microphysical characteristics of the observed cloud. These low droplet concentrations are critical regarding our understanding of the role of condensational inertia as pointed out in Section 4.1.

To address the reviewer's question as to whether there is truly a condensational "bottleneck" for cloud droplet numbers as low as those reported here, it seems the corresponding marine stratocumulus research regarding ultra clean layers (Wood et al., 2018; Kuan-Ting O et al., 2018) might be most relevant. Laminar veil clouds that detrain from marine cumulus can persist on the order of hours against very weak lift (1 cm s^{-1}). While containing drop effective radii in excess of 20 μm, the persistence of these clouds (timescales on the order of hours) against such weak updrafts suggests weak sedimentation and little collision-coalescence activity else clouds would more quickly dissipate. Subsequent modeling results (Kuan-Ting O et al., 2018) indicate that little if any sedimentation and collision coalescence persists after parcels moved into the detrained quiescent layer. Finally, DSD solutions for marine aerosol populations in vigorous (cumulus) updrafts have already been demonstrated to asymptote to an upper effective radius below 20 μm with diminishing dispersion and spectral width magnitudes above cloud base for a polydisperse parcel model (Pinsky et al., 2014), indicating that without broadening and/or collision-coalescence mechanisms, there is a definite upper limit to the size of droplets produced through condensational growth alone. Regardless, we have removed the "bottleneck" vocabulary from the revised manuscript and just directly refer to a narrow, large drop, condensational mode.

It is hard for me to understand why it is important that the cloud is supercooled. Wouldn't the same physics affect warm layer clouds?
In short, yes, the same physics apply in warm cloud layers. But consider for a moment marine StCu. Such clouds are BL phenomena occurring over a flat surface. There appear few if any drivers for SCVVFs to occur within the middle of these clouds. In such cases, vertical velocity fluctuations that can act to enhance drizzle production will almost certainly be confined to cloud top and therefore it should not be surprising that drizzle initiation occurs at the top of these cloud layers.

However, the emphasis here on a supercooled cloud must consider that: (1) this cloud had extremely cold cloud tops (T~-30°C), which Demott et al. (2010) suggest should lead to high INP concentrations, so the near absence of ice is quite surprising; and (2) for supercooled mixed phase clouds to produce SCDD requires relatively few CCN and INP. This scenario all but requires that supercooled clouds be inefficient precipitators with most of the mass distributed in the SLW categories. This also means that nearly all supercooled drizzling clouds can be expected to respond in kind to SCVVFs/Overturning Cells, which have already been acknowledged to be nearly ubiquitous in an orographic environment.

Condensational Inertia and Conceptual Model

R1: To me the correlation between Ncld and w' looks poor - can you plot scatter plots and give correlation coefficients - or even do lagged correlations given the discussion at the end of the paper?

R2: The schematic diagram presented in Fig. 13 is interesting, but I believe that the condensational inertia theory of why the LWC and Nd estimates are not in quadrature is insufficient. As the authors argue, the condensational delay may be around 10 seconds (phase relaxation timescale), yet the time between wave crests is substantially longer than this (probably 100 s or more for wind speeds of 10-20 m/s and wavelengths of 1-2 km).

Both referees indicated a desire for better quantification of the relationship between w' and CWC'/N_{cld}'. For referee 1 this had to do with some suggested N_{cld}/CWC relationship while for referee 2 it concerned the time/spatial scales and the lack of time series signals being in the expected quadrature relationship as per the proposed conceptual model (Fig. 13). To examine these relationships more quantitatively, the higher (5 Hz) resolution w', CWC', and N_{cld}' time series for were detrended and filtered of frequencies smaller than 0.1 Hz (wavelengths longer than 1 km). These time series were lagged by 0.2 s increments over a full 10 s period and correlated with a Pearson autocorrelation function to determine the correlation coefficients at each time lag. The results are presented below:

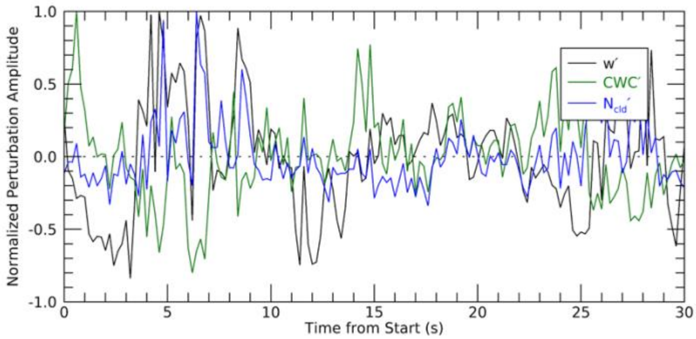

Figure 1: Normalized perturbation time series for selected kinematic and microphysical measurements. Measurements have been de-trended and filtered of frequencies lower than 0.1 Hz (corresponding to wavelengths longer than ~1 km).

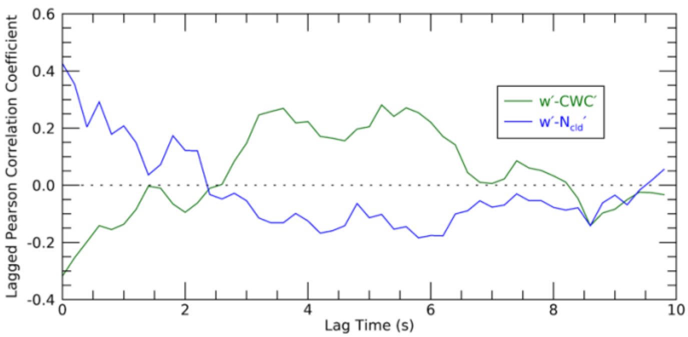

Figure 2: Lagged Pearson correlation coefficients for the time perturbation quantities in Fig. 1.

The lagged correlations (with maxima at position 0) clearly indicate that these condensational kinetic responses are zero-lag, with w'-CWC' being anticorrelated and w'-N_{cld}' positively correlated. Zero-lag correlations in this context likely indicate that cloud parcels are moving with(in) the kinematic pattern as opposed to through it as the latter should result in some spatial lag corresponding to the motion of parcels relative to w' pattern. This analysis has led us to modify the conceptual model presented in the original conceptual model with a more simple one. The analysis, while discrediting the original model, otherwise strengthens the suggested microphysical response. Furthermore, for the phase relaxation time to have led to a spatial lag exactly in quadrature now seems obviously unlikely, and we thank the referees for asking us to quantify these relationships. A new conceptual model incorporating this insight is proposed with perturbations caused from kinetic responses to a vertical velocity couplet more closely resembling the overturning cells suggested in HM05 to avoid the flow continuity issues that arise from this vertical parcel motion framework (e.g. when considering the location of maximum vertical displacement of parcels).

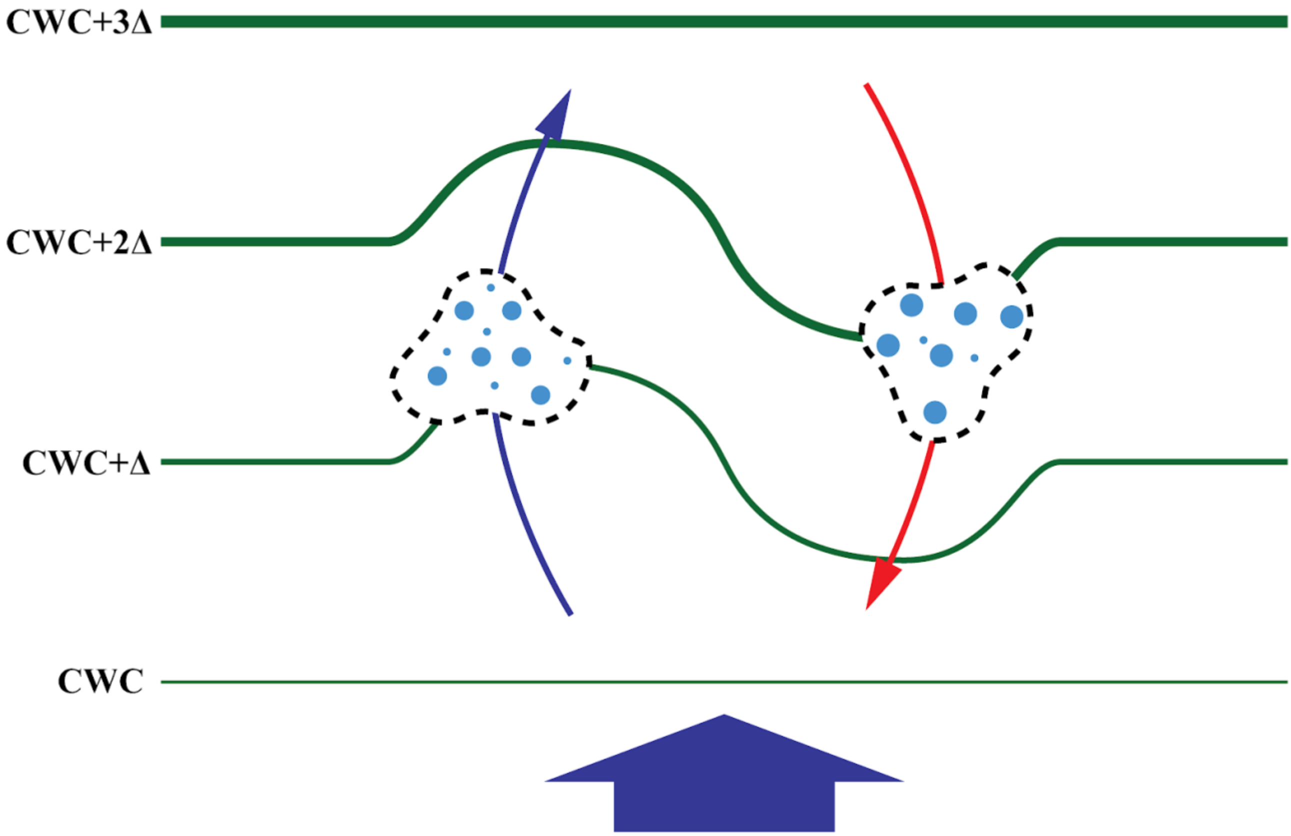

Figure 3: Revised conceptual model: simplified schematic of spatial responses to the perturbation updraft (blue) and downdraft (red) pattern superimposed on broader orographic lift (broad blue arrow bottom). The colored trajectories indicate the approximate path of parcels passing through the kinematic pattern following the schema of Houze and Medina (2005). Lines of constant cloud water content (green) indicating the expected deformations due to condensational kinetic effects, with line weight corresponding to relative condensate mass. Cloud parcels circulate within the vertical velocity perturbation pattern and more and smaller drops are located in perturbation updrafts than downdrafts. CWC contours appear flat and unperturbed above and below the vertical velocity fluctuation pattern as they are determined by the adiabatic ascent in the broader uplift pattern.

References

DeMott, P. J., A. J. Prenni, X. Liu, S. M. Kreidenweis, M. D. Petters, C. H. Twohy, M. S. Richardson, T. Eidhammer, and D. C. Rogers, : Predicting global atmospheric ice nuclei distributions and their impacts on climate, Proc.Natl.Acad.Sci.USA, 107, 11217-11217-11222, https://doi.org/10.1073/pnas.0910818107, 2010.

Houze, R. A. and S. Medina: Turbulence as a Mechanism for Orographic Precipitation Enhancement, J.Atmos.Sci., 62, 3599-3599-3623, https://doi.org/10.1175/JAS3555.1, 2005.

Kuan-Ting, O., R. Wood, and C. S. Bretherton: Ultraclean Layers and Optically Thin Clouds in the Stratocumulus-to-Cumulus Transition. Part II: Depletion of Cloud Droplets and Cloud Condensation Nuclei through Collision–Coalescence, J.Atmos.Sci., 75, 1653-1653-1673, https://doi.org/10.1175/JAS-D-17-0218.1, 2018.

Majewski, A. J., 2019: Supercooled Drizzle Drop Development In a Postfrontal Orographic Layer Cloud in Response to Semi-Coherent Vertical Velocity Fluctuations, University of Wyoming. https://search.proquest.com/docview/2282179118

Pinsky, M., I. P. Mazin, A. Korolev, and A. Khain: Supersaturation and diffusional droplet growth in liquid clouds: Polydisperse spectra, J.Geophys.Res.Atmos., 119, 12,872-12,872-12,887, https://doi.org/10.1002/2014JD021885, 2014.

Wood, R., K. O, C. S. Bretherton, J. Mohrmann, B. A. Albrecht, P. Zuidema, V. Ghate, C. Schwartz, E. Eloranta, S. Glienke, R. A. Shaw, J. Fugal, and P. Minnis: Ultraclean Layers and Optically Thin Clouds in the Stratocumulus-to-Cumulus Transition. Part I: Observations, J.Atmos.Sci., 75, 1631-1631-1652, https://doi.org/10.1175/JAS-D-17-0213.1, 2018.

Supercooled Drizzle Development in Response to Semi-Coherent Vertical Velocity Fluctuations Within an Orographic Layer Cloud

Adam Majewski[1], Jeffrey R. French[1]

[1]Department of Atmospheric Science, University of Wyoming, Laramie, 82070, USA

Correspondence to: Adam Majewski (amajewsk@uwyo.edu)

Abstract. Observations of super~~-~~cooled liquid water are nearly ubiquitous within wintertime, orographic layer clouds over the intermountain west; however, observations of regions containing super~~-~~cooled drizzle drops (SCDDs) are much rarer and the factors controlling SCDD development and location less well understood. As part of the Seeded and Natural Orographic Wintertime clouds—the Idaho Experiment (SNOWIE) goal of improving understanding of natural cloud structure, this study examines the role of fine-scale (sub-kilometer) vertical velocity fluctuations on the microphysical evolution and location of SCDDs within the observed mixed-phase, wintertime orographic clouds from one research flight in~~of~~ SNOWIE. For the case examined, ~~This flight saw~~ SCDDs developed in an elevated, postfrontal layer cloud with cold cloud tops (T < -30 °C)~~—containing~~ and low number concentrations of both ice (less than ~~N_{ice} <~~ 0.5 L^{-1}) and cloud droplets (less than ~~N_{cld} <~~ 30 cm^{-3}). Regions of supercooled drizzle at flight level extended more than a kilometer along the mean wind direction and were first located at and below layers of semi-coherent vertical velocity fluctuations (SCVVFs) embedded within the cloud and subsequently below cloud top. The microphysical development of SCDDs in this environment is catalogued using size and mass distributions derived from in ~~-~~situ probe measurements. Regions corresponding to hydrometeor growth are determined from radar reflectivity profiles retrieved from an airborne W-band cloud radar. Analysis suggests that SCVVF layers ~~(e.g. from K-H waves)~~ are associated with local SCDD development in response to the kinematic perturbation pattern. This drizzle development and subsequent growth by collision-coalescence is inferred from vertical reflectivity enhancements (-20 dBZ ~~/~~km^{-1}), with drizzle production confirmed by in ~~-~~situ measurements within one of these SCVVF~~vertical velocity fluctuation~~ layers. The SCDD production and growth occurs embedded within cloud over shallow (km or less) layers before transitioning to drizzle production at cloud top further downwind, indicating that wind shear and resultant vertical velocity fluctuations may act to enhance or speed up~~be more important for~~ SCDD development compared to classic~~than~~ cloud top broadening mechanisms in ~~the~~ orographic (or similarly sheared) cloud environment(s).

1 Introduction

Over the last forty years, there have been numerous field campaigns either directly or indirectly examining mixed-phase, orographic layer clouds over the intermountain western United States (Hobbs, 1975; Cooper and Saunders, 1980; Heggli and Reynolds, 1985; Rasmussen et al., 1992; Ikeda et al., 2007; Rosenfeld et al., 2013). At cloud-top temperatures between 0 and -20 °C, these clouds frequently contain extensive regions of Supercooled Liquid Water (SLW), especially near cloud top, making such clouds a prime meteorological environment for aircraft icing (Hindman et al., 1986; Ashenden et al., 1996; Marwitz et al., 1997). In some instances, SLW mass may be distributed entirely across cloud droplets, those liquid hydrometeors that are relatively small and have not attained appreciable fallspeeds, taken to have diameters less than 50 µm for the purpose of this study. On the other hand, ~~Supercooled dD~~drizzle~~ Drizzle~~ d~~D~~rops~~ (SCDDs)~~, with diameters~~ are the~~ 50 to ~~-~~500 µm, ~~supercooled drops which~~ have appreciable ~~(0.1-2 m/s)~~ fall velocities (0 to 2 m s^{-1}) relative to cloud droplets ~~(D < 50 µm) motions~~ and can consequently grow rapidly ~~in diameter~~ via ~~collision~~ collision-coalescence in the presence of cloud droplets (~~dD/dt ~ exp(t);~~ Lamb and Verlinde, 2011). Supercooled drizzle drops (SCDDs) are of special concern in aircraft icing, because of the collection and subsequent freezing of these drops on aircraft wings aft of de-icing devices, such as pneumatic boots (Ashenden et al., 1996). This study aims to catalogue the effect of local, kilometer-scale kinematic perturbation patterns on the development and location of SCDDs for one such mixed-phase cloud system.

R~~Most r~~ecent climatologies (Rauber et al., 2000; Bernstein et al., 2007) describe SCDD development as occurring predominantly through~~by~~ collision-coalescence growth in supercooled clouds largely devoid of ice hydrometeors~~completely supercooled liquid clouds~~. Studies explicitly examining the microphysical development of SCDDs with in ~~-~~situ aircraft data confirmed the primacy of the collision-coalescence growth mechanism (Cober et al., 2001) as opposed to the "classical" mechanism—which sees ice hydrometeors melt as they fall through an embedded warm layer (T > 0 °C) before subsequent supercooling as fully melted drizzle drops. Wintertime orographic layer clouds are frequently too shallow and too cold (outside of cold air damming events on the east coast of the U.S.) to support a warm nose (Rauber et al., 2000)—therefore the climatologies suggest that ~~collision~~ collision-coalescence is the dominant SCDD development mechanism in the clouds of interest in this study.

Collision-coalescence growth is favored in clouds with low cloud droplet number concentrations. For clouds with similar condensate supply rates, those with ~~populations of~~fewer cloud droplets will more quickly produce droplets of larger diameter ~~reach~~ large ~~condensational "bottleneck"~~ (D ~ 30-40 µm) that approach sizes with appreciable terminal fall velocities, subsequently stimulating further growth through collision-coalescence compared to~~faster than~~ clouds with more numerous droplets. For this reason, clouds formed in clean air masses (i.e. with lower numbers of cloud condensation nuclei; CCN) or in less vigorous updrafts (where saturation ratio remains nearer unity ~~S* is nearer 1 and~~ with fewer activated CCN ~~are activated~~) are kinetically favored for drizzle formation (Freud and Rosenfeld, 2012). In agreement, the conditions of limited CCN abundance and gradual ascent are linked to high frequency of SCDD observation ~~formed via collision-coalescence at a climatologic scale~~ (Rauber et al., 2000; Bernstein et al., 2007). Regions which see shallow clouds form from warm, moist air gradually lifted over an arctic cold front or orography frequently see SCDD formation—faster and more extensively if the clouds form in clean, maritime air masses (Rasmussen et al., 2002). A region that has uplift mechanisms in both orography and surface frontal passage, as well as the required cloud level moisture supply, is the American InterMountain West (IMW) during the winter storm season.

The presence and amount of ice act as~~provides~~ additional~~nother~~ factors influencing~~precondition for~~ SCDD development in mixed phase orographic clouds. ~~, as the (bulk) i~~Ice phase hydrometeors typically acquire~~s~~ mass more rapidly than ~~the~~ liquid species~~phase~~ owing to both a greater~~n increased~~ diffusional vapor pressure gradient ~~($e_{si} < e_i$)~~ and increased individual linear growth rates due to crystal geometry and riming. This places an upper limit on active ice nucleating particle (INP) and ice crystal number for SCDD formation, else ice will more rapidly scavenge the available vapor and cloud water, inhibiting growth of cloud droplets to drizzle sizes (Rasmussen et al., 2002; Geresdi and Rasmussen, 2005). A byproduct is that SCDD observations are infrequent in clouds with cloud tops colder than -15 °C, with few ~~if any~~ observations of SCDD formation found in the literature with cloud tops colder than -20~~3~~ °C (Lawson et al. 2001; Korolev et al., 2002; Rosenfeld et al., 2013; Silber et al., 2019). ~~In the shallow orographic layer clouds of interest to this study, cloud top temperatures are typically warmer than -20 °C when not part of a deeper precipitating frontal structure, limiting natural primary ice nucleation.~~

Collision-coalescence initiation and growth often~~further~~ depend~~s~~ on broadening mechanisms for the largest ~~bottleneck~~ droplets to begin collection of smaller droplets in the population in all but the cleanest of clouds (Wood et al., 2018), and this is true regardless if clouds are supercooled~~. (via fall speed separation)~~. Steady condensational growth alone ~~is responsible for distribution~~ leads to a narrowing of the drop size distribution (DSD) around a~~the~~ large drop mode (D ~ 30-40 µm~~) bottleneck diameter~~, ~~so drop size distribution (~~such that DSD~~)~~ broadening mechanisms (e.g. turbulent or isobaric mixing, eddy hopping, etc.) are necessary to provide the differential fall speed conducive to collision-coalescence onset and subsequent rapid collectional growth. Pobanz et al. (1994) found that when ~~Observational results of~~ SCDDs formed in clouds with ~~greater~~ cloud droplet number concentrations of more than ~~(N_{cld} >~~ 100 cm^{-3}~~), indicated that~~ layers of cloud top shear were correlated with vertical location of drizzle development~~ in cloud~~, presumably due to turbulent broadening or mixing~~this mechanism (Pobanz et al., 1994)~~. Shear-induced turbulent mixing, ~~(~~especially at cloud top,~~)~~ is thought to be responsible for relatively rapid DSD~~drop size distribution~~ broadening (Grabowski and Abade, 2017). Any isobaric mixing of different temperature parcels near the cloud boundary (e.g. for clouds with a strong capping ~~cloud top~~ inversion) are expected to further accelerate this process. This is why the warm rain process is understood to start at or near cloud top, with drizzle mass principally increasing with cloud layer depth (Comstock et. al., 2007).

Supersaturation history provides an analytical framework for understanding several ~~of these broadening~~ mechanisms (e.g. vertical velocity fluctuations, turbulent eddy hopping, mixing events, etc.) that~~which~~ may be responsible for the rapid spectral broadening and subsequent collision-~~-~~coalescence enhancement~~behavior~~ in warm stratiform clouds (Cooper et al., 1989; Korolev and Mazin, 1993; Politovitch and Cooper, 1994; Korolev, 1995). For instance, Korolev found that when modeled cloud parcels are subjected to repeated vertical velocity fluctuations, DSDs~~drop size distributions~~ broaden and may even see a second, small-diameter droplet mode develop from interstitial CCN activation (hereafter, secondary droplet activation). Turbulence and wave motions were both suggested as possible ~~meteorological~~ sources for these vertical velocity fluctuations, but the lack of parcel-following in ~~-~~situ measurements made validating these behaviors an observational challenge (Pobanz et al., 1994).

Between the orographic SLW case studies (Rauber and Grant, 1986; Rauber 1992), SCDD climatologies (Rauber et al., 2000; Bernstein et al. 2007), mechanistic understandings of SCDD production (Rosenfeld et al. 2013), and exceptional cases (Korolev and Isaac, 2000; Pobanz et al., 1994), a clear picture of SCDD formation develops: clouds formed in gradual updrafts within~~by~~ low CCN and INP populations ~~in gradual updrafts will~~ are most likely to produce SCDD. The frequency, spatial extent, and thermodynamic extremity of SCDD production is a function of ~~absolute~~ CCN and INP abundance (Rosenfeld et al., 2013). Wind shear and dynamic instability appear to lead to SCDD development in clouds with exceptionally high CCN concentrations given low enough ice concentrations (Korolev and Isaac, 2000; Pobanz et al., 1994). Mixed-phase~~Supercooled~~ clouds throughout the western U.S. in which the phase partitioning is mostly liquid~~with mass distributed toward mostly SLW categories~~ are ~~not un~~common even well away from the coast (Hindman, 1986). Such clouds must contain low concentrations of~~in~~ cloud droplets and ice to develop SCDDs (Saleeby, 2011). Where encountered in orographic environments ~~(e.g. coastal mountains)~~, these supercooled, relatively clean clouds are expected to encounter vertical and turbulent motions at both broad and fine scales (Houze and Medina, 2005).

~~Whatever the development mechanism, studies have reported SLW in orographic mixed-phase clouds across the entire IMW region (Cooper and Saunders, 1980; Rauber and Grant, 1986; Rauber, 1992; Rosenfeld et al., 2013), with amount and spatial extent decreasing primarily due to number of upstream barriers (Hindman, 1986; Saleeby et al., 2011). Observational and modeling results confirm that the frequency of SCDD development and collision-coalescence activity within larger SLW pockets is linked to both low CCN and INP concentrations (Rasmussen et al., 2002; Rosenfeld et al., 2013). The comprehensive climatology of Bernstein et al. (2007) agreed with the gradient expected SCDD frequency gradient based on earlier case studies, with the highest SCDD frequency maximum extending along the Pacific coastal barrier mountains (in WA, OR, and CA), otherwise showing a decreasing SCDD frequency with distance inland from the Pacific across the IMW. This reaffirms the expected link between climatologically clean air masses and SCDD formation (Rauber et al., 2000), however observations (Korolev and Isaac, 2000) and models (Rasmussen et al., 2002) demonstrate the possibility of SCDD development in *both* maritime and continental air masses given low enough ice number and active cloud top broadening mechanisms. Rosenfeld et al. (2013) clarified this aerosol-precipitation relationship for the region, demonstrating that frequent passage of maritime airmasses (i.e. low CCN and INP concentration) is associated with a higher frequency of SCDD development, greater in-cloud SCDD spatial extent, and persistence of SCDD to more extreme thermodynamic conditions (e.g. cloud top temperature < -20 °C) relative to continental air masses. Modeling results have confirmed that for maritime (continental) air masses, freezing drizzle development is faster (slower) due to lesser (greater) CCN concentrations and occurs over a deeper (shallower) layer near cloud top; however, both situations require ice crystal concentrations less than about 0.08 L^{-1}, at least in models (Rasmussen et al., 2002). According to the expectations of both the IMW climatology~~

~~and the drizzle formation mechanism, understood from modeling and observations, freezing drizzle frequency and in-cloud spatial extent is expected to decrease with distance from the Pacific across the IMW.~~

This study examines an individual case from a field campaign located in the IMW~~southwest Idaho~~ in which~~that saw~~ SCDDs develop~~ed~~ed~~ment~~ in a~~n~~ winter orographic cloud system despite cold cloud tops (T $\sim$~~<~~ -3~~2~~0 °C) which are typically associated with more active ice nucleation and more abundant natural ice (DeMott et al., 2010). ~~The p~~Persistently low droplet number concentrations (~~75th percentile of N~~cld~~CDP~~ less than~~cloud observations below~~ 50 cm^{-3}~~-~~) ~~for 12 of 23 flights)~~ and frequent SCDD observations from about half of the cases throughout the field campaign~~(13 of 23 flights)~~ (Tessendorf et al., 2018) inspired this analysis and are~~seem~~ consistent with the climatological maxima of wintertime SCDD frequency that stretches from the coastal barrier mountains into Idaho (Bernstein et al., 2007). The analysis focuses on the spatial kinematic patterns and their effect on the liquid phase precipitation development in these mixed phase clouds.

2 Study Area and Data

The Seeded and Natural Orographic Wintertime clouds—the Idaho Experiment (SNOWIE) was designed to observe and analyze the evolving wintertime orographic cloud structure in a series of prescribed airborne cloud seeding experiments (Tessendorf et al., 2018). As part of this process, it was necessary to establish the evolution of the natural cloud structure and microphysics as a baseline for evaluating cloud seeding effects. Separately,~~A separate objective was to use~~ the extensive dataset and state~~-~~-of~~-~~-the~~-~~-art measurements were expected to yield ~~to arrive at~~ new insights toward~~s understanding~~ the natural cloud structure, microphysical evolution, and precipitation patterns of mixed phase winter orographic clouds~~, independent of cloud seeding effects~~. Understanding how ~~fine~~ fine-scale (km or less) dynamical processes impact ~~the~~ cloud microphysical development and spatial distribution, amount, and phase, of observed precipitation in such~~these~~ clouds is at~~on~~ the forefront of ~~observational work undertaken in~~ the remote sensing and cloud microphysics observational literature~~communities~~ (e.g. Houze and Medina, 2005) and further provides valuable insight to cloud modeling and microphysical parameterizations.

To characterize and describe the development of precipitation hydrometeors (e.g. SCDDs) at flight level requires ~~knowledge of the~~ direct measurements of~~instantaneous~~ cloud hydrometeor spectra~~um~~, ~~current~~ thermodynamic and dynamic conditions (which~~ in part~~that govern the development of th~~e~~is ~~spectrum~~spectra), and characterization of the spatial variability of each~~these parameters~~. Remote profiling radar, in -situ cloud probes, temperature and humidity sensors, and gust probes, onboard~~To catalogue cloud structure and precipitation evlution,~~ the University of Wyoming King Air (UWKA) research aircraft catalogued the evolving cloud structure and precipitation patterns for ~~over~~ ~~equipped with remote profiling radar, cloud probes, temperature and humidity sensors, and a gust probe~~ repeated fixed flight legs oriented along the mean wind direction through cloud (Fig. 1), at as low an altitude as practical. UWKA legs, ~~were~~ anchored above the Packer John (PJ, see Fig. 1) ground site, ~~to~~ recurrently sampled ~~nearly~~ coincident ~~the same~~ spatial cross sections through the evolving orographic cloud structure, often between the -10 to -15 °C level~~isotherms~~. Flight legs (blue line in Fig. 1) were generally no longer than 100 km, with the western end located over the valley and the eastern end extending over the Sawtooth Mountain Range. ~~Bulk thermodynamic and dynamic atmospheric conditions were characterized by~~ S~~s~~oundings launched at Crouch, ID (KCRH, Fig. 1) before ~~(~~and during~~)~~ each flight were used to characterize~~d~~ bulk thermodynamic and dynamic conditions. ~~Legs were generally no longer than 100 km, with the western end located over the Payette Valley and the eastern end over the Sawtooth Mountain Ranges.~~

Measurements from ~~T~~SNOWIE ~~utilized t~~the W-Band Wyoming Cloud Radar (WCR) ~~to~~ documented the orographic cloud structure above and below flight level and provided context for the in ~~-~~situ cloud microphysics measurements (as in Vali et al., 1998; Wang and Geerts, 2003; Wang et al., 2012). Previous studies demonstrated that the WCR ~~could~~ resolves ~~fine~~ fine-scale details of orographic clouds (~30 m spatial resolution), observing aspects of their dynamical and microphysical structure technologically impossible in previous decades (Aikins et al., 2016). The ~~(95 GHz frequency) of the~~ WCR is sensitive to cloud droplets and drizzle in the Rayleigh regime, with Mie effects starting at around 600 μm and reflectivity increasing monotonically with diameter up to millimetric sizes (D > 0.95 mm). Radar reflectivity for volumes containing even large drizzle drops was therefore dominated by the contribution of the largest drops, and throughout SNOWIE~~as~~ no ~~SCDD~~ drizzle drops larger than 0.5 mm diameter were observed such~~so~~ that ~~larger~~~~with diameters greater than about 0.5 mm (diameter) over the course of SNOWIE based on examination of particle images captured by in situ probes,~~ Mie effects were non-existent for purely liquid volumes. ~~Additional pulse-pair~~ Doppler velocity measurements from the WCR captured the near-vertical, reflectivity-weighted motions of the distributed hydrometeor targets. In the data presented here, no attempt has been made to separate hydrometeor terminal fall velocity with vertical air motions. Since the antennas point nearly vertical, the influence of horizontal wind in the Doppler measurements is negligible for straight and level flight. ~~after correction to remove any projection of the horizontal wind into the beam pointing direction.~~

In situ probes on the UWKA measured cloud hydrometeors with diameters from a few microns to several millimeters ~~in size~~ (Table 1). Two probe types were used to collect these data—a forward scattering cloud probe (i.e. the Cloud Droplet Probe, CDP), and two optical array probes (OAPs) for larger hydrometeors ~~(D > 50 μm)~~. The CDP (Lance et al., 2010) provided 5 Hz cloud droplet (1 to 50 μm) size spectra in bins 1 to 2 μm wide. The CDP RMS accuracy of mean droplet diameter of 0.7 μm was determined after the campaign using the University of Wyoming droplet generator (Faber et al., 2018).

The OAPs~~,~~ ~~on the other hand,~~ image~~d~~ larger hydrometeors (D > ~50 μm) as ~~the~~ particles pass through an illuminated sample volume and shadow individual members of a linear photodiode array. The 2D Stereo p~~P~~robe (2DS; Lawson et al., 2006) imaged particles at a 10 ~~-~~μm resolution across a 1.28 mm diode array, accurately resolving the hydrometeor spectra for particles 50 μm < D < 1 mm~~illimeter~~. The 2D Precipitation p~~P~~robe (2DP) measured hydrometeors larger than a millimeter with an image resolution of 200 μm. The data from the OAPs were processed using the University of Illinois OAP Processing Software (Jackson et al., 2014, Finlon et al., 2016), to perform standard image rejection and dimension corrections. ~~Size distributions were produced from i~~Image-derived size and particle timing information and a ~~calculated~~ sample volume estimate ~~— estimated from particle diameter, true airspeed, laser wavelength, and particle acceptance criteria~~ ~~(~~following Heymsfield and Parrish (1978) were used to produce particle size distributions. Shattering artifacts were~~by large~~

~~ice crystals was~~ avoided using anti-shattering tips on the 2DS and by filtering of particles with a short, static inter-arrival time threshold in the software processing.

From these 1 Hz particle size spectra~~distributions~~, several integrated water content metrics were calculated to estimate the ~~instantaneous~~ mass distribution within certain drop size categories~~ of interest~~. The total liquid water content—i.e. across the entire measured liquid hydrometeor size spectrum~~—LWC~~ was integrated from the combined CDP and 2DS size spectra and is hereafter referred to as LWC_{tot}.~~ under the assumption of no SLW drops larger than the 1.3 mm upper size limit of the 2DS, based on visual inspection of probe images~~[1]. The Cloud Water Content (CWC) and Drizzle Water Content (DWC) metrics contain the mass from the 2 to ~~-~~50 µm and 50 µm to ~~-~~1~~.3~~ mm parts of the cloud hydrometeor spectrum, respectively, and hence sum to LWC_{tot}. The calculated LWC_{tot} was compared to the bulk estimate from the Rosemount~~Rosemont~~ icing probe, which is ~~(also~~ sensitive to all sizes of SLW drops.~~ with of D > 50 µm.)~~ A comparison performed over two flight~~over two mostly liquid~~ legs ~~from the research flight to~~ validated these estimation methods. The only remarkable disagreement between the metrics came for LWC values of the Rosemount~~Rosemont~~ greater than~~above~~ 0.4 g~~/~~ m^{-3}, where the integrated LWC_{tot} was~~became~~ larger compared to the Rosemount~~Rosemont~~ icing probe measurement. This may be an overestimation of LWC_{tot}~~may be~~ related to mis-sizing~~ed~~ of drizzle drops that are near the edge of the depth-of-field in the 2DS and appear as hollow images. Conversely, this may also be due to an underestimation from the Rosemount probe due to splashing of SCDDs that are not completely captured by the probe's icing rod. Regardless, the error is almost certainly associated with the liquid mass of SCDDs and the Rosemount and the integrated LWC_{tot} estimates provide a lower and upper bound, respectively.~~particles with D >over 50 µm in diameter (i.e. imaged, drizzle-sized donuts and partial donuts), corroborated by a similar departure of the RosemountRosemont from the integrated CWC for these same high LWC values, suggesting that the disagreements were caused by drizzle-sized particles (missed in the CWC and overestimated in the LWC~~$_{tot}$~~). While other potential sources of measurement error exist (particularly for the RosemountRosemont probe), both the estimates integrated from the CDP and 2DS for these high LWC points err in the direction suggestive of mis-sizing of drizzle drops, making it the likely error source~~.

The following results and analysis produced from the WCR profiles, in-situ bulk probes, and cloud microphysics datasets from the first UWKA flight in SNOWIE, highlight~~s~~ the role of sub-kilometer vertical velocity fluctuations on the spatiotemporal distribution of SCDDs and the inferred cloud microphysical response.

3 Results

The results presented are from the period of 0245 to 0405 UTC (legs 1, 2, and 5) during the first flight of the field campaign on January ~~7-~~8, 2017. Two distinct layer clouds developed in the wake of a precipitating frontal cloud system. Of these two clouds, the elevated cellular cloud layer contained both low background number concentrations of ice and cloud droplets and embedded kilometer or longer regions of SCDDs that formed in a larger pattern of orographic lift.

3.1 Synoptic and Thermodynamic Context

The UWKA research flight followed the passage of a deep snow band associated with a weak jetstreak in the 500 mb wind field~~ (not shown)~~. The deep, saturated atmosphere present in the upstream sounding during the heavily-precipitating period ~~(~~roughly 4 hours prior to the start of leg 1~~ start;~~ (Fig. 2a), experienced mid-tropospheric drying, and veering and strengthening of the winds above 8 km MSL. This led to lowered cloud tops and a pronounced dry slot from 7 to 9 km in the pre-flight sounding just 3 hours later ~~(~45 min prior to leg 1 start, ~~(Fig. 2b). This dry layer contained thin layers of expected dynamic instabilities—defined by bulk Richardson number from 0 to 0.5 (Fig. 2b; blue shading). The layer below, between 4 and 7 km, saw several vertical humidity variations accompanied by evaporational cooling of the radiosonde upon exiting cloud layer tops, resembling conditional instabilities (orange shading). These layers were not expected to correspond to real convective motions in cloud.

By the start of the first flight leg at 2:45 UTC, a shallow orographic cloud layer persisted over the study region~~Payette basin~~ on the western end of the flight track, with cloud tops around 4 km MSL (Fig. 3a)—matching the top of the lower saturated layer in the pre-flight sounding (Fig. 2b). This orographic cloud layer was capped on the eastern end by a layer of broken, cellular cloud structures roughly 1 to ~~-~~3 km wide—hereafter the elevated cellular layer—resembling, at times, either coherent K-H billows or incoherent generating cells. This elevated cellular layer was consistently strongest ~~(~~in terms of layer depth and highest radar reflectivities~~)~~ over the highest terrain at the east end of the leg.

The final upstream sounding launched one hour after the start of leg 1 (Fig. 2c~~); ~1 hour after leg 1 start)~~ indicated a deeper saturated layer through 6.5 km and further strengthening and veering of the wind above, with more vertically homogeneous, near-zonal winds between 3 and 6 km. This shear profile resulted in several layers of possible~~indicated~~ dynamic instability~~ies~~ within ~~the ~~500 m both above and below the top of the saturated layer and matched well with the 6 to 6.5 km cloud tops observed ~~in ~~with the WCR during flight legs 4 and 5 (~~nearest in time; ~~Fig. 3d and ~~/~~3e).

Variations in humidity and wind, superimposed on the background zonal winds and low-level orographic clouds, appeared responsible for an elevated cloud layer that was at times ~~dynamically ~~unstable and variable in vertical location and depth (Fig. 2b). Additionally, a surface inversion and attendant low-level static stability was present in all the upstream soundings around the time of the flight (Fig. 2a, b and ~~-~~c). As a result, calculated bulk Froude numbers were consistent with blocked flow below 2 km MSL~~ (not shown)~~, matching the overall low-level static stability pattern that was present through much of the ~~entire ~~field campaign (Tessendorf et al., 2018). The stability from this surface inversion may have helped to decouple the surface airmass from the free troposphere above the Sawtooth Range~~Payette Mountains~~ barrier.

3.2 General Cloud Structure and Vertical Motions

There were several differences between the orographic cloud layer (4.5 km MSL and below) and the cellular layer above. The orographic cloud layer persisted over the nearest 1 to ~~-~~2 km above the terrain, with cloud tops that rose slightly (no more than 500 m) from west to east with the average height of the topography beneath (e.g. Fig. 3a). The cellular layer, however, was transient—discrete layers of cells advected into the target area at varying altitudes. Some of these layers appeared coupled to the lower orographic cloud layer (as in legs 1, 2, 4, and 5), while others appeared totally separate (as in legs 3, 9, and 10). This behavior is consistent with the large vertical variations in wind shear and humidity between the three soundings in this layer (Fig. 2), including several dynamically unstable layers. Consistent with this, several of the elevated layers appeared to contain overturning (or breaking) cells in the reflectivity profiles, for example, within the elevated cellular layer of leg 4 from 10 to ~~-~~15 km downwind of PJ (Fig. 3d).

Across the entire research flight, the radar reflectivity within the upper cloud layer was~~maintained reflectivities~~ less than -5 dBZ except for discrete, ~~outside of~~ individual fall streaks~~, which remained discrete as they advected across the flight track~~. This behavior suggests~~ed~~ mostly liquid cloud species in the elevated layer, confirmed by the 99^{th} percentile of precipitation-sized ice number (integrated from the 2DP probe) for each of the first four legs remaining below 0.1 L^{-1} ~~(~~and for leg 5 ~~was~~ only marginally higher, with a 99^{th} percentile value of 0.3 L^{-1}~~)~~. Some of the higher reflectivity fall streaks, ~~(~~especially towards the end of the flight,~~)~~ may have corresponded to seeding lines (French et al., 2018; Tessendorf et al., 2018; Hatt ~~et al.~~, 2019) after the seeding period started at the end of leg 2, but are otherwise beyond the scope of this study~~do not warrant any further consideration beyond noting the location and effect of ice on observed reflectivities and size distributions~~. The radar reflectivity~~ies~~ within the lower orographic cloud layer, by comparison, was~~were~~ greater than in the cellular layer above.~~, with~~ Large regions ~~whole sections~~ within ~~of the nearest~~ 1 km of the surface contained reflectivity greater than~~AGL of cloud above~~ 5 dBZ, suggesting the presence of ice below the orographic cloud top~~ (or interface)~~. This conjecture is consistent with a significant reduction of about 4 m s^{-1} in downward Doppler velocity in the lowest ~1 km above the surface (Fig. 4). This reduction often occurred at a level corresponding to an increase in the radar reflectivity. The inferred relative abundance of ice in this shallow orographic layer may be due to more abundant aerosol (and INP) presumed to reside below the strong surface inversion (Fig. 2b) or from secondary ice multiplication in the warm (-5 < T < -15 °C) temperatures in the lower layer, but no direct in situ measurements were available in cloud below flight level.

Mean reflectivity-weighted, near-vertical Doppler velocities (hereafter, hydrometeor vertical velocities or Doppler velocities) were available from the WCR to quantify cloud vertical motions (i.e. the convolution of vertical *air* motions and reflectivity-weighted population *terminal* *fall speed*~~velocity~~). ~~Additional corrections were applied to remove the contributions by the horizontal wind for profiles where the radar beams deviated from vertical.~~ Unfortunately, ~~the~~ complex dynamics at~~down to~~ sub-kilometer scales and~~convoluted with~~ hydrometeor size and phase inhomogeneity convoluted~~confounded~~ the observed Doppler velocities, making assumptions about a constant hydrometeor fall speed specious. In fact, the spread of fall speeds associated with observed hydrometeor size distributions ~~and phase variations — from the negligible fall speeds of populations of cloud droplets to the 1 m/s or more fall speeds of drizzling populations —~~ were greater than the spread of air motions observed in the dynamic structures of focus (< 1.5 m~~/~~ s^{-1} amplitude where sampled at flight level).

Despite this complexity, there were several obvious and consistent trends in the observed Doppler velocities: nearly all legs showed a distinct terrain-induced vertical velocity couplet centred roughly 24 km downwind of Packer John and directly above a pronounced N-S ridge, oriented perpendicular to the mean wind and flight direction (Fig. 4). This couplet consisted of up to 2 m~~/~~ s^{-1} upward Doppler velocities over the upwind slope immediately followed by as much as 4 m ~~/~~s^{-1} downward Doppler velocities on the downwind side, and frequently extended up to cloud top (as in leg 5). Despite the wave-like signatures present in the reflectivity profiles, Doppler velocity couplets ~~(~~away from flight level, ~~)~~ and phase relationships ~~(~~at flight level, ~~)~~ between perturbation kinematic and thermodynamic quantities (not shown) were inconsistent with K-H waves. For this reason, care was taken separately in (1) quantifying the effects of spatial variations in hydrometeor fall speed ~~spatial variation~~ and (2) adopting the label of semi-coherent vertical velocity fluctuations (SCVVFs) to distinguish layers of these regularly-spaced, oriented vertical velocity perturbations from the more isotropic turbulent motions found elsewhere. Probable meteorological sources for SCVVFs in this environment include K-H waves, shear-driven mechanical overturning (Houze and Medina, 2005), and shallow convective overturning with some regular triggering mechanism; however, the actual sources did not seem to uniquely affect the microphysics and therefore remain undistinguished. What follows are descriptions of how ~~these~~ SCVVFs affected the evolution and spatial distribution of precipitation in the~~is~~ elevated cellular cloud layer, significant for where drizzle development deviated from the expectation of starting at cloud top and collecting through the depth of ~~whole~~ SLW cloud ~~layer~~.

3.3 Comparisons Between Drizzling Legs (1, 2, and 5)

The three flight legs of interest, ~~legs~~ 1, 2, and 5 (Table 2), were flown at altitudes ranging from 3.9 to ~~-~~4.5 km MSL. During each of the legs the UWKA~~, each~~ encounter~~ed~~ed kilometer-or-longer stretches of SCDD measured at flight level within the elevated cellular cloud layer. ~~, with s~~Significantly larger drops were observed on the first two legs compared to leg 5 despite similar cloud water contents across all three. The~~se~~ regions containing SCDDs were all located at or downwind of Packer John mountain (PJ; the start of prominent terrain features along this transect), where reflectivities and cloud layer thicknesses were consistently near the leg maxima ~~(leg 4 being the lone exception)~~. Above the windward slope of the Sawtooth Range, from 10 to ~~-~~25 km downwind of PJ, was a broad region of ascent observed on most legs (0 to ~~-~~1 m ~~/~~s^{-1} hydrometeor upward velocities) which contributed to the relatively high reflectivities and cloud layer thicknesses compared to cloud further upwind (Fig. 4). From 10 to ~~-~~60 km downwind of PJ, where SCDDs were encountered on all three legs ~~(the regions of interest for SCDDs)~~, flight level vertical velocities ~~for the three legs~~ varied from -0.5 to 2 m ~~/~~s^{-1}, with perturbation magnitudes on legs 1 and 2 of up to 0.6 m ~~/~~s^{-1} and less~~entirely lower~~ than 0.2 m ~~/~~s^{-1} for leg 5 (Table 2). The~~se legs sampled altitudes from 3900-4500 m, corresponding~~ flight level ~~to~~ temperatures on these legs ranged from ~~as low as~~ -16 °C ~~(~~on legs 2 and 5~~)~~ to -11 °C ~~(~~for the lowe~~st~~r altitude leg 5~~)~~.

~~The sampled~~ Cloud Water Content (CWC) ~~values~~ measured at flight level~~by the CDP~~ were ~~very~~ similar for these drizzling sections of cloud across all three flight legs, with maximum values approaching 0.6 g ~~/~~m^{-3} in ~~both~~ legs 1 and 5. ~~— the more widespread SCDD extent and occasionally broken cloud conditions of~~ Slightly lower maximum CWCs were measured in the drizzling sections of leg 2, only ~~saw CWC~~ as high as 0.4 g ~~/~~m^{-3}, possibly reduced due to scavenging and removal of cloud water by drizzle in the time between legs 1 and 2 (Table 2). Cloud droplet number concentration measured at flight level during all three ~~for these~~ legs never exceeded~~remained below~~ 35 cm^{-3}~~, the observed maxima for this research flight,~~ and decreased to values less~~lower~~ than 5 cm^{-3} within portions of cloud in which there appeared~~with~~ significant SCDD sedimentation from above~~ (as in legs 1 and 2), where both cloud and drizzle drops appeared to be the largest~~. Within t~~T~~hese plumes of SCDDs, which appeared only in flight legs 1 and 2, DWC measured at flight level were at times as high ~~-plumes contained as much~~ as 1 g ~~/~~m^{-3}~~ liquid water distributed over drizzle sizes (i.e. DWC, D > 50 μm)~~. Also within SCDD plumes, the mean-volume diameter of the DSD ~~Total spectral MVD's for these SCDD plumes~~ approached 80 μm (Table 2). Unlike the first two legs, the SCDDs sampled in leg 5 were much smaller, and the DSD mean-volume diameter did not exceed ~~with MVD only approaching~~ 45 μm.~~, even within the plumes.~~

The primary microphysical differences for these three legs were the smaller SCDDs in leg 5 relative to legs 1 and 2. The following section provides an ~~detailed~~ analysis of where ~~these~~ SCVVFs may have acted to enhance~~led to rapi~~d hydrometeor growth and the subsequent evolution of cloud downwind~~ and with time~~.~~A further cloud kinematic structural difference is the focus of the following section.~~

3.4 Semi-Coherent Vertical Velocity Fluctuations

The primary structural difference within~~between~~ the elevated cellular cloud layer across~~for~~ these three legs, which appeared responsible for cloud microphysical characteristics~~differences in cloud droplet size~~ and SCDD ~~vertical level of~~ development, were the presence and vertical location of layers of ~~semi-coherent vertical velocity fluctuations (~~SCVVF~~'~~s~~)~~. A train of these velocity fluctuations were sampled at flight level during leg 1 from 24 to 35 km downwind of PJ~~the first leg and illustrate the cloud microphysical response~~ (Fig. 5). T~~Here, from 24 to 35 km downwind of PJ, t~~he SCVVFs appeared as a series of ± 0.5 m ~~/~~s^{-1} vertical velocity perturbations ~~from the mean~~ with a wavelength of roughly 1 to ~~-~~2 km~~ wavelength~~ (Fig. 5b). The vertical velocity fluctuations drove both a thermodynamic (Fig. 5e) and microphysical response (Fig. 5c and ~~/~~d), which saw positive perturbation vertical velocities paired with lower temperatures, higher cloud droplet number, and lower CWC relative to the mean trend. Appreciable drizzle mass was only present in the perturbation downdrafts (Fig. 5c, pink curve). From~~When~~ ~~averaged~~ size distributions averaged across~~were examined for~~ individual perturbation up- and downdrafts (Fig. 6), it i~~wa~~s apparent that secondary droplet activation was primarily responsible for the increased droplet number concentration within perturbation updrafts. DSD~~The averaged size distribution~~s corresponding to ~~positive~~ perturbation updrafts show that much of the increased droplet number concentration can be explained by an increased~~the large~~ number of 6 to ~~-~~8 μm droplets, which are an order of magnitude more abundant than within the perturbation~~interspersed~~ downdrafts and nearly as abundant as the number of droplets in the primary mode from 25 to ~~-~~35 μm. Given that these legs were flown at a constant altitude, the secondary droplet activation in perturbation updrafts, paired with a reduction in the~~lower~~ CWC~~ than the trend~~, may indicate kinetically limited parcel behavior and is examined in the discussion. The perturbation downdrafts contained increased ~~drizzle mass (i.e.~~ DWC~~)~~, larger droplets, and lower total number concentration relative to perturbation updrafts. The decreased number and increased DWC are likely explained by scavenging by the larger drops, which were as large as 150 μm (Fig. 6), and indicate an active collision-coalescence process~~es at flight level~~. Furthermore, collision-coalescence likely began very near or just above flight level, as the reflectivity values were between -25 and -15 dBZ within the nearest 400 m above flight level are ~~,~~ indicative of populations of cloud droplets with very few, if any, drizzle drops (Fig. 5a).

Spatiotemporal ~~profiles~~ cross-sections of Doppler velocity (Fig. 7) highlight the difficulty in identifying layers of SCVVFs away from the aircraft using the WCR. During leg 1, ~~Near flight level~~ from 25 to ~~-~~30 km downwind of PJ, a region where in situ measurements~~where the gust probes~~ indicate~~d~~ a regular perturbation velocity pattern with 1 to ~~-~~2 km spacing (~~dashed line,~~ Fig. 5~~7~~b), there appears~~is~~ no similar Doppler~~hydrometeor vertical~~ velocity pattern from the WCR within the nearest few hundred meters of flight level~~from the WCR gates to the UWKA~~ (Fig. 7a). However~~For comparison~~, within ~~the nearest~~ 200 m of~~to~~ cloud top, from~~between~~ 30 to ~~-~~35 km downwind of PJ, ~~the top of~~ a clear train of ~~these~~ vertical velocity fluctuations can be seen (Fig. 7a). These Doppler velocity fluctuations match the crests of the wavelike reflectivity structures near cloud top in the corresponding reflectivity profile (Fig. 5a, top circled), but do not extend as far downward into cloud as the reflectivity structures. This perturbation velocity pattern is clearest in the highest 200 m of cloud, presumably ~~in part~~ due to the smaller sizes and resulting lower terminal velocities of ~~populations of~~ scatterers there. In regions lower in cloud, ~~compared to~~ the radar volumes contain more and larger~~ing~~ drizzle drops and the resulting ~~below, where the~~ Doppler velocities become gradually more negative, eventually dominating the overall Doppler velocity pattern. ~~as the drizzle drops begin to dominate the reflectivity and where reflectivity-weighted terminal fall velocities become greater than the air motions.~~ Very near flight level, it is possible to ~~A similar increase in~~ *estimate*~~d~~ *the hydrometeor terminal fall speed* ~~reflectivity-weighted terminal velocities – this time estimated from comparing flight level gust probe and near-aircraft Doppler velocities –~~ by subtracting the in situ measured air velocity from the WCR measured Doppler velocity in the nearest range gates. Near~~occurred at~~ flight level, 29 km downwind of PJ, we note an increase in hydrometeor terminal velocity (Fig. 7b, red and blue lines). This ~~,~~ matches~~ing~~ ~~where a sharp increase in estimated fall speed is noted from SCDD falling from aloft. This matches~~ well with ~~the~~ increases in DWC~~drizzle mass~~ and DSD mean volume diameter~~spectral MVD~~ beginning at nearly the same location illustrated in Fig. 5 c and e.~~time (blue arrow, Fig. 5c/e), both indicating SCDD falling from aloft~~.

The link between SCVVFs and hydrometeor growth is~~was~~ also apparent in ~~the~~ Contoured Frequency by Altitude Diagrams (CFADs) generated from~~of~~ WCR radar reflectivity measurements. For the region in leg 1 corresponding to the sampled SCVVF train at flight level, ~~(~~25 to ~~-~~30 km downwind of PJ~~;~~ (Fig. 8a), the median reflectivity rapidly increased from a roughly constant -25 dBZ above 5 km MSL (~500 m above flight level) to greater~~higher~~ than -15 dBZ just below flight level, suggesting rapid growth ~~– consistent with a transition~~ from cloud droplets ~~(D < 30 µm)~~ to drizzle drop sizes for the low ~~(N < 35 cm^{-3})~~ number concentrations observed in these clouds. This increase was characterized by a roughly -20 dBZ ~~/~~km^{-1} slope in the reflectivity CFAD which appeared consistently within ~~the~~ layers of SCVVFs elsewhere in cloud this day. For example, in~~, e.g. where~~ a layer of ~~these~~ SCVVFs near~~appeared at~~ cloud top at 6 km MSL, located ~~(~6 km MSL)~~ at 30 to 35 km ~~in the next 5 km of cloud~~ downwind of PJ, a similar reflectivity slope with altitude is measured (Fig. 8b). The reflectivity enhancement tied to both of these layers of SCVVFs i~~wa~~s discrete, in comparison to the more gradual growth (roughly -7 dBZ km^{-1}) that occurred further~~est~~ downwind on this leg, starting at cloud top and extending through the entire cloud layer (Fig. 8c).

The ~~result~~ impact that ~~of these layers of~~ SCVVF layers had on the broader microphysical character of ~~sampled~~ cloud during~~for~~ leg 1 was a trend of increasing hydrometeor size with distance downwind. At the location of broad 0.5 to ~~-~~1 m ~~/~~s^{-1} updraft ~~-from~~ 20 to ~~-~~25 km downwind of PJ (Fig. 5b), the DSD~~cloud hydrometeor size spectrum~~ contained mostly~~resembled a population of strictly~~ cloud droplets with diameters less~~almost entirely smaller~~ than 40 µm (~~outside of the overestimation in the 2DS curve beyond the discontinuity;~~ Fig. 9a, red). In the region of SCVVFs ~~-~~at flight level ~~immediately further downwind (~~25 to ~~-~~35 km downwind of PJ~~)~~, the ~~primary modal~~ diameter of the cloud droplet mode shifts to larger sizes and~~while~~ the steep exponential tail ~~toward large sizes simultaneously~~ flattens out into a drizzle shoulder (Fig. 9a, green and blue). Even f~~F~~urther downwind (Fig. 9a, orange and purple), ~~of the SCVVF train,~~ a mature drizzle shoulder (100 µm < D < 300 µm) becomes apparent. Here, downwind of the SCVVFs at flight level, the sampled drizzle ~~from SCDD's falling~~ originates from the layer near cloud top. ~~These SCVVF layers appear to be responsible for the trend of increasing drop size with distance – as layers of SCVVFs formed over prominent terrain elements, hydrometeor growth was enhanced and drop sizes increased below and downwind of these layers.~~

Observations from flight ~~L~~leg 2 indicate~~saw~~ that the SCVVF layers present in~~from~~ leg 1 had broken~~break~~ down into incoherent turbulence. ~~between legs, with the elevated cellular layer containing~~ A~~a~~ prominent drizzle precipitation plume was present from 45 to ~~-~~53 km downwind of PJ, capped by a turbulent and variable cloud top height (circled, Fig. 10a). Still present were juxtaposed perturbation updrafts and downdrafts, especially near cloud top (Fig. 10b), but these were not well-organized nor layered as observed in leg 1 and did not have a unifying spatial scale. Within t~~T~~he ~~circled~~ drizzle plume clearly evident in the~~in the~~ reflectivity field (Fig. 10a), in situ measurements revealed DWCs in excess of~~revealed agreed with the~~ 0.4 g ~~/~~m^{-3} ~~or higher DWC where the 0 dBZ and higher reflectivities crossed flight level~~ (Fig. 10d). While several short wavelength perturbations appeared in the flight level vertical velocity profile (Fig. 10c), the~~rey did not have a~~ did not appear a consistent correlation~~effect~~ ~~on~~ for ~~the~~ either the thermodynamic (Fig. 10e) or the bulk microphysical measurements ~~data~~ (Fig. 10d), unlike leg 1.

Leg 5, by comparison, contained a long~~er~~ and~~,~~ shallow~~er~~ layer of SCVVFs located ~~-from~~ 12 to ~~-~~33 km downwind of PJ between 4.5 and ~~-~~4.8 km MSL, about ~~and~~ 500 to ~~-~~1000 m below cloud top (Fig. 11a, circled) and just above the flight level. The horizontal scale of these fluctuations was smaller than in leg 1, with the width of a complete up/down perturbation couplet less~~narrower~~ than 1 km ~~for this SCVVF train~~ (Fig. 11b). Perhaps because of both the ~~relatively~~ thinness of the SCVVF layer ~~of these SCVVFsSCVVF's~~ and its nearness to flight level ~~(only 750 m above flight level)~~, drops were much smaller compared to those observed in leg 1. The DSD mean volume diameter~~and the spectrum MVD~~ remained below 45 µm (Table 2) and ~~. Averaged~~ size distributions at flight level just below these SCVVFs~~SCVVF's~~ reveal significantly lower concentration of drizzle drops with D > 100 µm compared to those observed in both legs 1 and 2~~a indicated mostly small drizzle drops with diameter just greater than 50 µm, some larger ice hydrometeors toward millimetric sizes~~ (Fig. 9c). Unlike observations in legs 1 and 2 however, there did appear~~and~~ a relatively even partitioning of mass distribution between CWC and DWC (Fig. 11d)~~, unlike legs 1 and 2~~. Also, t~~T~~he presence of ice was corroborated by 2DS probe images (not shown) indicating that any vertical reflectivity enhancements from layers of SCVVFs~~SCVVF's~~ for this leg are complicated by the increased linear growth rates (and hence reflectivity response) of ice in a mixed phase environment.

Reflectivity and Doppler velocity CFADs for three 5 km-wide drizzling columns from legs 1, 2, and 5 were generated for comparison (Fig. 12). The incoherent turbulence at cloud top for leg 2, seen in the large spread of Doppler velocities in the highest 1 km of cloud (Fig. 12e), produced a similar vertical reflectivity enhancement pattern as in the e~~E~~astern end of leg 1 (Fig. 8c), where reflectivity gradually increases~~d~~ with distance downward ~~over~~ through the elevated cellular layer. This pattern also appears in drizzling marine stratocumulus clouds where drizzle production typically occurs at cloud top and drizzle drops grow throughout the entire cloud layer (e.g. Comstock et al., 2007~~5~~). T~~For both drizzling columns, t~~he broadening processes associated with incoherent turbulence and entrainment at cloud top are~~were~~ sufficient for drizzle production and subsequent ~~collectional~~ accretional growth through the whole cloud layer. By comparison, the thin embedded layer of SCVVFs present in leg 5 led to a shallow growth layer with larger reflectivity-altitude gradients (i.e. more horizontal slope in the thinner shaded growth region; Fig. 12g) than in either legs 1 or 2. The larger ice particles present in the tail of the corresponding size distribution for the column from leg 5 (Fig. 9c~~; confirmed by 2DS images – not shown~~) explain the similar median radar reflectivity up to ~~values (-5 to~~ 0 dBZ~~)~~ at~~crossing~~ flight level observed in ~~between~~ legs 2 and 5 (Fig. 12 d and ~~/~~g) despite the comparatively smaller, more numerous drizzle drops in leg 5 compared to legs 1 and 2. All three drizzling columns contained reverse S correlation patterns between reflectivity and Doppler velocity in the vertical, associated with hydrometeor growth and fallout over the layer (Fig. 12 c, ~~/~~f, and ~~/~~i).

4 Discussion

Much of the previous work describing SCDD development in orographic, mixed phase cloud systems focused on the necessary conditions for development—namely the low cloud droplet and ice number concentrations coupled with ~~and sufficient~~ condensate supply rates sufficient to support condensational growth to the droplet sizes required for active collision-coalescence (Rauber, 1992; Ikeda et al., 2007). Several other studies suggest~~ed~~ conditions which may be responsible for accelerated drizzle development or for relaxing these necessary conditions, introducing broadening mechanisms important for SCDD production in cloud (Pobanz et al., 1994; Korolev and Isaac, 2000). Of these, the relationship between fine wind shear levels, spatial supersaturation fluctuations, and SCDD development has yet to be connected mechanistically by in-situ measurements, despite being identified both as associated with SCDD development (Pobanz et al., 1994) and, separately, as important for the spectral broadening seen in certain layer clouds (Cooper, 1989; Korolev, 1995; Korolev and Mazin, 1993). The observations here seem an important continuation of the work by Pobanz et al. (1994), which called for further airborne research investigating the link between layers of strong wind shear and SCDD development. While their explanation called for observations of K-H billows to understand the production mechanisms, the microphysical behavior in layers of SCVVFs here seems to provide similar insight towards understanding these mechanisms.

4.1 Microphysical Response to SCVVF Layers

The insight provided from sampling one of these SCVVF trains with the in-~~-~~situ cloud hydrometeor probes (Fig. 5) allows for some characterization of the microphysical processes in clouds of this type. Based on the flight level measurements ~~microphysical and kinematic data~~, a conceptual model is presented to consistently describe the microphysical response to SCVVF~~ layer~~s (Fig. 13). The kinematic structure and LWC response for leg 1 saw positive (negative) perturbation updrafts (downdrafts) paired with negative (positive) C~~L~~WC perturbations from the trend and positive (negative) cloud droplet number concentration perturbations associated with droplet activation (evaporation). For these regular vertical velocity fluctuations in clouds ~~(and~~ with sufficiently low concentrations of cloud droplets~~N_{cld}~~ ~~$_{CDP}$)~~, the supersaturation response to vertical velocity fluctuations as described by Korolev (1995), is responsible for (re-)activating interstitial CCN as small (6 to ~~-~~8 µm) droplets in the sub-adiabatic perturbation updrafts and separately broadening the primary ~~bottleneck~~ droplet mode from ~~the~~ repeated supersaturation fluctuations. Sub-~~-~~adiabatic implies LWC values below what is expected from the adiabatic LWC formulation,

$$LWC = \Gamma_{LWC} \cdot (z - z_{CB}), \qquad (1)$$

where Γ_{LWC} represents the adiabatic lapse rate of liquid water content determined by cloud base temperature and pressure (Albrecht et al., 1990) and z - z_{CB} is the height above cloud base. The mean CWC for the SCVVFs sampled~~train seen~~ at flight level was 0.25 g ~~/~~m^{-3} with regularly spaced oscillations ± 0.05 to ~~-~~0.08 g ~~/~~m^{-3} about~~from~~ that mean (Fig. 5c).

In a well-mixed (i.e. nearly constant equivalent potential temperature; Fig. 2), non-precipitating orographic layer cloud, ~~the expectation is that for a constant altitude,~~ the adiabatically-constrained C~~L~~WC is expected to remain~~be~~ nearly constant at a given altitude, with only small perturbations that are the result of variations in ~~the~~ cloud base thermodynamic conditions~~, i.e. P_{cb} and T_{cb}~~. Back of the envelope calculations estimate the specific adiabatic C~~L~~WC lapse rate of this elevated cellular layer cloud is~~to be~~ about~~round~~ 0.001 g ~~/~~m^{-4}, taking the thermodynamic conditions from the sounding at the interface between the orographic and elevated cellular layers as a pseudo cloud base for this upper layer. Given ~~the~~ mean CWC~~cloud water contents~~ of 0.25 g ~~/~~m^{-3} observed at flight level, this indicates roughly 250 m of ascent for the cloud parcels sampled at this altitude. Variations of ±5 °C at cloud base would then correspond to ±0.05 g ~~/~~m^{-3} perturbations in C~~L~~WC, and variations of ±50 mb would correspond to ±0.01 g ~~/~~m^{-3} perturbations, respectively. While the orographic environment does predispose clouds to experience more variation in cloud base conditions than similar layer clouds associated with fronts or boundary layers, cloud base thermodynamic variations of this magnitude are not expected over~~at this~~ spatial scales of ~~(~~0.5 to ~~-~~2 km~~)~~ and are therefore insufficient to explain~~do not likely explain~~ the regular CWC perturbation observed~~response~~. Instead, the perturbations of up to 40% of the mean CWC at a constant altitude were likely the result of dynamic and/or precipitation processes that were tied to the SCVVFs~~and not the cloud thermodynamics~~.

The primary effect on ~~LWC – or, more aptly,~~ CWC if only condensational effects are considered and where drizzle is not falling through parcels from above may be explained ~~—~~due to ~~cloud kinematics is~~ the kinetic effect as described by Korolev (1995). The negative CWC perturbations in leg 1 were accompanied by local supersaturation sufficient for secondary droplet activation (i.e. saturation ratio large enough to activate interstitial CCN~~S>S*>1~~), inferred from the presence of small droplets (6 to ~~-~~8 µm) ~~mode present in the averaged size distributions~~ within ~~these~~ perturbation updrafts (Fig. 6a, red and blue curves). Such sub-adiabatic behavior is~~seems~~ linked to the kinetic limitation on condensational growth. As noted earlier, ~~—cloud parcels had low enough (N_{CDP} < 15 cm^{-3})~~ cloud droplet number concentrations were less than 30 cm^{-3} and ~~that~~ the "condensational inertia" of droplet populations to~~in~~ condense~~cing~~ ~~out~~ excess ~~supplied~~ water vapor supply governed the supersaturation response, associated CWC response, and secondary droplet activation behavior. For the droplet populations less than~~below~~ 30 cm^{-3} and ~~with~~ mean count diameter of between ~~roughly~~ 20 and ~~-~~30 µm, the corresponding phase relaxation time is around 10 s (using estimation methodology by Fukuta and Walter, 1970; Polotivitch and Cooper, 1988; and Korolev, 1995). This phase relaxation time corresponds to expected perturbations from the adiabatic mean of as much as 0.02 g ~~/~~m^{-3} at flight level, ~~which~~ indicating~~e~~ that, while the kinetic effect cannot fully explain the ~~full~~ perturbation magnitude in the CWC field, it acts in the proper observed direction and explains the primary adiabatic (i.e. closed parcel) effect in these clouds. This zero-lag anticorrelation between vertical velocity~~w~~ and CWC perturbations results in the spatial pattern illustrated in Fig. 13. ~~Compared to quiescent clouds, those(without devoid of SCVVFs,) there are more active DSD broadening processes and larger CWC gradients coincident with regions of probable turbulent mixing, which appear to explain the observation that initial SCDD production can be enhanced byis linked to these SCVVF layers. It is important to note, that while CWC would be maximized at maximum parcel displacement for *instantaneous* condensation, the condensational inertia represents a spatiotemporal lag displacing these maxima (minima) into the perturbation downdrafts (updrafts), as illustrated in Fig. 13.~~

The remaining magnitude of CWC variation is likely ~~seems to be~~ related to ~~either~~ the precipitation dynamics~~ or the breakdown of the "well-mixed" assumption implicit in the vertically-stratified adiabatic cloud model~~. ~~In the first case, r~~Removal of cloud water by scavenging from drizzle in perturbation updrafts would lead to lower CWC~~'~~s and reduced cloud droplet number~~(and Ncld's) than expected from the kinetic-adiabatic model alone~~. While the lower CWCs are indeed observed, and this may account for the greater magnitude reduction expected from the~~ the~~ kinetic-adiabatic model alone, cloud droplet number concentrations increase. However, the increase in activation due to the kinetic limitation as noted previously is likely greater than the reduction in number concentration due to scavenging. Within the i~~I~~nterspersed perturbation downdrafts, greater DWC and ~~see~~ larger drizzle drops are observed, indicating active collision-coalescence. CWC and cloud droplet number concentrations are therefore expected to be further depressed relative to the mean than expected from the kinetic condensational effect alone. These regions ~~and more drizzle mass (consistent with the observed DWC pattern; Fig. 5c) and~~ are the likely ~~the~~ origin of drizzle fall streaks observed in the WCR profiles~~in the vertical~~ and ~~is~~ are represented by slightly larger drizzle drops in the downdraft region in Fig. 13.~~ In the second case, if the perturbation velocity structure is sufficiently long-lived, for the long phase relaxation times here, the regular vertical velocity pattern may act to advect or deform the local vertical CWC stratification. In this case, at a constant altitude, observed perturbation updrafts would contain lower CWC advected from below which has yet to mix out with surrounding parcels or adjust via condensation. In this case, the vertical CWC contour deformations required to explain the remaining 0.03 to -0.067 g /m-3 of~~

~~CWC perturbation would be on the order of 30 to -70 m and require the kinematic pattern to persist for 1 to 21-3 minutes given the relatively weak perturbation vertical velocity of magnitudes (±0.2 to -0.5 m/s-1.) — which seems unrealistic.~~

4.2 Reflectivity-Inferred Hydrometeor Growth in SCVVF Layers

C~~The c~~omparisons between vertical reflectivity, Doppler velocity, and their cross correlation suggest two main microphysical behaviors within layers of SCVVFs~~semi-coherent vertical velocity fluctuations~~. The first is rapid, and often discrete, drop growth in the vertical tied to layers of vertical velocity fluctuations and~~,~~ not confined to cloud top. This vertical growth rate appears as large for these SCVVF layers in leg 1 as for the drizzle production at cloud top in leg 2~~, with similar observed LWC's and liquid-ice mass distribution (unlike leg 5)~~. The second behavior is a reverse S cross correlation pattern (cf. Vali et al., 1998) in~~for these~~ layers of SCVVFs, irrespective of hydrometeor phase differences, which further corroborates the local hydrometeor growth and fallout tied to these ~~vertical~~ layers.

Layers of SCVVFs in legs 1 and 5 were responsible for vertical reflectivity enhancements similar in magnitude~~, (~ ~~ roughly -20 dBZ ~~/~~km^{-1}~~,)~~ as produced by the drizzling cloud in leg 2 where layers of SCVVFs were not present. However, these SCVVF layers, ~~(~~especially in the relatively upwind cloud elements closer to PJ,~~)~~ were responsible for discrete growth layers ~~of growth~~ that did not begin at~~were not confined to~~ cloud top~~ (Fig.'s 9a/10g)~~. This indicates that the vertical velocity fluctuations were likely responsible for the initiation of collision-coalescence and drizzle production which~~and~~ occurred earlier~~faster~~ and at a different location in cloud compared to the ~~than~~ classic~~al~~ idea of~~warm rain~~ production at cloud top. ~~broadening mechanisms (i.e. turbulent entrainment, isobaric mixing, etc) which~~ F~~f~~urther downwind, corresponding to ~~or~~ later in time from the upwind edge, ~~were sufficient for~~ drizzle production and growth did occure~~continued~~ at cloud top and subsequent growth of the SCDDs occurred through the depth of the~~over the whole~~ SLW layer, even without the presence of SCVVFs. This was most apparent in the transition between legs 1 and 2 from discrete growth at the level of these SCVVFs to growth over the entire layer, starting at cloud top, in leg 2. While ~~only a~~ qualitative~~ observation~~, this observation suggests the importance of ~~warrants an examination of~~ SCVVFs in other layered liquid cloud~~ regime~~s where embedded shear or shallow layers of static instabilities may be responsible for enhancing~~the vertical initiation of~~ the collision-coalescence process. Layers of SCVVFs may also be important in clouds where condensational growth and cloud top spectral broadening occur~~s~~ too slowly for active warm rain production, although with the caveat that any condensational kinetic effects are bound to be smaller than reported here. This, however, agrees with the observations of both Pobanz et al. (1994) and Korolev and Isaac (2005).

A distinct feature of the layers of SCVVFs~~semi-coherent vertical velocity fluctuations~~ is the bimodal DSD with populations of large (D > 30 µm) and small (D < 10 µm) droplets of similar number, not present elsewhere in cloud. This small droplet mode contains ~~does not contain~~ much less mass compared to the large droplet mode, and collisions between the large and small droplets are likely inefficient (E ~ 1 to ~~-~~3% for drops of these sizes in laminar flow; Rogers and Yau, 1996), but the effect of such numerous possible collision events, ~~(~~especially given the large fall speed separations,~~)~~ in a turbulent environment may be enough to break the colloidal stability of the ~~bottleneck~~ narrow large drop mode for a few lucky drops~~,~~

such that subsequent self-collection within this mode becomes favored. Furthermore, parcel model results (Korolev 1995) have shown repeated supersaturation variations driven by vertical velocity fluctuations ~~have been shown via parcel models to~~ produce a local broadening about the larger droplet mode ~~(Korolev 1995)~~. This broadening may provide enough fall speed separation for self-collection without the need for larger droplets to physically interact with the newly activated smaller droplets. The~~and agrees qualitatively with~~ increases in drop size and drizzle mass with distance downwind within SCVVF~~the vertical velocity fluctuation~~ layers where parcels ~~may be expected to~~ have undergone repeated ~~more~~ supersaturation fluctuations are in qualitative agreement with this hypothesis.

A~~The second apparent phenomenon — a~~ reverse S ~~vertical~~ cross~~-~~correlation pattern between reflectivity and Doppler velocity with altitude across these SCVVF~~growth~~ layers ~~—~~further corroborates the drop growth in these layers~~ of vertical velocity fluctuations~~. Vali et. al (1998) demonstrated t~~T~~his pattern in drizzling coastal stratus~~, where it appeared in drizzling coastal stratus (Vali et al., 1998), was suggested to be~~ as the result of upward transport of drizzle and dilution of downward moving parcels near cloud top (region of positive correlation) which transitioned to the dominance of precipitation terminal fall speed increases ~~velocity effects~~ below (region of negative correlation). Here the same trend is present in leg 5 (Fig. 12g), where the very low background reflectivities (-25 dBZ) above the growth layer transition to rapid reflectivity increases below 5 km MSL correlated with positive Doppler velocities (Fig. 12i). As the Doppler velocities become more negative below this layer (Fig. 12h), the pattern reverses to the falling drizzle (and ice) dominating the reflectivity signature—with strong~~ly~~ anticorrelation~~negative correlations~~ between reflectivity and Doppler velocity. This~~e~~ strong~~ly~~ anti~~negative~~ correlation ~~between reflectivity and Doppler velocity in this region~~ is dominated by the terminal fall speed~~velocity~~-size relationship (e.g. terminal fall speed is proportional to the square of the diameter~~$v_T \sim D^2$~~ for drizzle drops)~~ where volumes with the largest particles have the most negative Doppler velocities and highest reflectivities~~. At the top of the growth layer, where ~~the~~ weaker positive correlation exists between reflectivity and Doppler velocity, it is important to consider both the contribution of hydrometeor terminal velocity and air motion to the observed Doppler velocities. For the populations just above the growth layer, terminal velocities for the largest ~~(D ~ 35 μm) bottleneck~~ cloud droplets are much less than the magnitude of the vertical velocity perturbations (±0.5 to -1.0 m ~~/~~s^{-1}) and therefore the Doppler velocity signal is dominated by ~~relative~~ air motions. This suggests that the regions of upward relative air motion are correlated with higher reflectivities near the top of ~~these~~ SCVVF layers, though without in~~-~~situ measurements nearer the top of these layers it is ~~not~~ impossible to determine~~ to indicate~~ whether this is due primarily ~~a~~ size or concentration~~ effect~~. A more expansive conceptual model (cf. Fig. 13) would incorporate the vertical gradient of these growth and fallout effects across the SCVVF layer but i~~wa~~s too conjectural without more penetrations through SCVVF trains at different altitudes.

5 Conclusions

Low cloud droplet number concentrations, less than ~~(Ncld$_{CDP}$ <~~30 cm^{-3}~~)~~, and precipitation-sized ice number concentrations, less than ~~(Nice$_{2DP}$ <~~ 0.5 L^{-1}~~)~~, despite cold cloud top temperatures (T ~~~~~ ≤ -30 °C), provided favorable conditions for the development of SCDD~~supercooled drizzle drop~~s ~~development~~ in a postfrontal orographic layer cloud forming over the Sawtooth Mountains in the American Intermountain West~~east of the Payette Basin~~. This cloud, while transient and variable in vertical location and depth, consistently was strongest over the prominent terrain features downwind of Packer John mountain, and frequently contained layers of ~~containing~~ SCVVFs~~semi-coherent vertical velocity perturbations~~. Where present~~ in the elevated cellular layer cloud~~, ~~layers of~~ SCVVFs were associated with local enhancement of the development and growth of SCDDs ~~development~~ in response to the kinematic perturbation pattern. This was demonstrated by strong~~ and rapid~~ vertical ~~reflectivity~~ enhancements in CFADs of reflectivity, on the order of ~~(~~-20 dBZ ~~/~~km^{-1}~~)~~, and attributed to ~~from~~ hydrometeor ~~collectional~~ growth through collision-coalescence. This drizzle production and growth occurred embedded within cloud and over relatively shallow layers before transitioning to drizzle production at cloud top and growth over the entire elevated cellular layer cloud. Compared to quiescent clouds, those ~~that contain~~containing SCVVFs will have more active DSD broadening processes and larger CWC gradients coincident with regions of probable turbulent mixing. This appears to explain the observation that initial SCDD production can be enhanced by SCVVF layers and can lead to SCDD production in vertical regions other than just cloud top.

Author Contributions

AM performed the analysis and prepared the manuscript. JRF contributed to interpretation of results and provided critical edits in preparing the manuscript.

Acknowledgements

Observations from and participation in the SNOWIE field campaign was funded through NSF grant AGS-1547101, with UWKA participation supported by NSF grant AGS-1441831. We would like to acknowledge the contributions of both Coltin Grasmick and Phil Bergmaier for both feedback on the ideas present herein and shared access of their IDL libraries used in several figures. Finally, the feedback and suggestions from the SNOWIE principal~~principle~~ investigators and senior scientists (Sarah Tessendorf, Lulin Xue, Kyoko Ikeda, and Roy Rasmussen of NCAR; Katja Friedrich of CU Boulder; and Bob Rauber of the University of Illinois) were invaluable in honing in on the important elements of this analysis.

References

Aikins, J., K. Friedrich, B. Geerts, and B. Pokharel: Role of a Cross-Barrier Jet and Turbulence on Winter Orographic Snowfall, Mon.Wea.Rev., 144, 3277-3277-3300, https://doi.org/10.1175/MWR-D-16-0025.1, 2016.

Albrecht, B. A., C. W. Fairall, D. W. Thomson, A. B. White, J. B. Snider, and W. H. Schubert: Surface-based remote sensing of the observed and the Adiabatic liquid water content of stratocumulus clouds, Geophys.Res.Lett., 17, 89-89-92, https://doi.org/10.1029/GL017i001p00089, 1990.

Ashenden, R., W. Lindberg, J. D. Marwitz, and B. Hoxie: Airfoil performance degradation by supercooled cloud, drizzle, and rain drop icing, Journal of Aircraft, 33, 1040-1040-1046, https://doi.org/10.2514/3.47055, 1996.

Bernstein, B. C., C. A. Wolff, and F. McDonough: An Inferred Climatology of Icing Conditions Aloft, Including Supercooled Large Drops. Part I: Canada and the Continental United States, J.Appl.Meteor.Climatol., 46, 1857-1857-1878, https://doi.org/10.1175/2007JAMC1607.1, 2007.

Cober, S. G., G. A. Isaac, and J. W. Strapp: Characterizations of Aircraft Icing Environments that Include Supercooled Large Drops, J.Appl.Meteor., 40, 1984-1984-2002, https://doi.org/COAIET>2.0.CO;2, 2001.

Comstock, K. K., S. E. Yuter, R. Wood, and C. S. Bretherton: The Three-Dimensional Structure and Kinematics of Drizzling Stratocumulus, Mon.Wea.Rev., 135, 3767-3767-3784, https://doi.org/10.1175/2007MWR1944.1, 2007.

Cooper, W. A.: Effects of Variable Droplet Growth Histories on Droplet Size Distributions. Part I: Theory, J.Atmos.Sci., 46, 1301-1301-1311, https://doi.org/EOVDGH>2.0.CO;2, 1989.

Cooper, W. A. and C. P. R. Saunders: Winter Storms over the San Juan Mountains. Part II: Microphysical Processes, J.Appl.Meteor., 19, 927-927-941, https://doi.org/WSOTSJ>2.0.CO;2, 1980.

DeMott, P. J., A. J. Prenni, X. Liu, S. M. Kreidenweis, M. D. Petters, C. H. Twohy, M. S. Richardson, T. Eidhammer, and D. C. Rogers, : Predicting global atmospheric ice nuclei distributions and their impacts on climate, Proc.Natl.Acad.Sci.USA, 107, 11217-11217-11222, https://doi.org/10.1073/pnas.0910818107, 2010.

Faber, S., J. R. French, and R. Jackson: Laboratory and in-flight evaluation of measurement uncertainties from a commercial Cloud Droplet Probe (CDP), Atmospheric Measurement Techniques, 11, 3645-3645-3659, https://doi.org/10.5194/amt-11-3645-2018, 2018.

Finlon, J. A., G. M. McFarquhar, R. M. Rauber, D. M. Plummer, B. F. Jewett, D. Leon, and K. R. Knupp: A comparison of X-band polarization parameters with in situ microphysical measurements in the comma head of two winter cyclones, Journal of Applied Meteorology and Climatology, 55, 2549-2549-2574, 2016.

French, J. R., K. Friedrich, S. A. Tessendorf, R. M. Rauber, B. Geerts, R. M. Rasmussen, L. Xue, M. L. Kunkel, and D. R. Blestrud: Precipitation formation from orographic cloud seeding, Proc.Natl.Acad.Sci.USA, 115, 1168-1168-1173, https://doi.org/10.1073/pnas.1716995115, 2018.

Freud, E. and D. Rosenfeld: Linear relation between convective cloud drop number concentration and depth for rain initiation, Journal of Geophysical Research: Atmospheres, 117,n/a, https://doi.org/10.1029/2011JD016457, 2012.

Fukuta, N. and L. A. Walter: Kinetics of Hydrometeor Growth from a Vapor-Spherical Model, J.Atmos.Sci., 27, 1160-1160-1172, https://doi.org/KOHGFA>2.0.CO;2, 1970.

Geresdi, I. and R. Rasmussen: Freezing Drizzle Formation in Stably Stratified Layer Clouds. Part II: The Role of Giant Nuclei and Aerosol Particle Size Distribution and Solubility, J.Atmos.Sci., 62, 2037-2037-2057, https://doi.org/10.1175/JAS3452.1, 2005.

Grabowski, W. W. and G. C. Abade: Broadening of Cloud Droplet Spectra through Eddy Hopping: Turbulent Adiabatic Parcel Simulations, J.Atmos.Sci., 74, 1485-1485-1493, https://doi.org/10.1175/JAS-D-17-0043.1, 2017.

Hatt, M.: Microphysical Impact of Cloud Seeding on Wintertime Orographic Clouds Observed During SNOWIE, University of Wyoming, 2019.

Heggli, M. F. and D. W. Reynolds: Radiometric Observations of Supercooled Liquid Water within a Split Front over the Sierra Nevada, J.Climate Appl.Meteor., 24, 1258-1258-1261, https://doi.org/ROOSLW>2.0.CO;2, 1985.

Heymsfield, A. J. and J. L. Parrish: A Computational Technique for Increasing the Effective Sampling Volume of the PMS Two-Dimensional Particle Size Spectrometer, J.Appl.Meteor., 17, 1566-1566-1572, https://doi.org/ACTFIT>2.0.CO;2, 1978.

Hindman, E. E.: Characteristics of Supercooled Liquid Water in Clouds at Mountaintop Sites in the Colorado Rockies, J.Climate Appl.Meteor., 25, 1271-1271-1279, https://doi.org/COSLWI>2.0.CO;2, 1986.

Hobbs, P. V.: The Nature of Winter Clouds and Precipitation in the Cascade Mountains and their Modification by Artificial Seeding. Part I: Natural Conditions, J.Appl.Meteor., 14, 783-783-804, https://doi.org/TNOWCA>2.0.CO;2, 1975.

Houze, R. A. and S. Medina: Turbulence as a Mechanism for Orographic Precipitation Enhancement, J.Atmos.Sci., 62, 3599-3599-3623, https://doi.org/10.1175/JAS3555.1, 2005.

Ikeda, K., R. M. Rasmussen, W. D. Hall, and G. Thompson: Observations of Freezing Drizzle in Extratropical Cyclonic Storms during IMPROVE-2, J.Atmos.Sci., 64, 3016-3016-3043, https://doi.org/10.1175/JAS3999.1, 2007.

Jackson, R. C., G. M. McFarquhar, J. Stith, M. Beals, R. A. Shaw, J. Jensen, J. Fugal, and A. Korolev: An Assessment of the Impact of Antishattering Tips and Artifact Removal Techniques on Cloud Ice Size Distributions Measured by the 2D Cloud Probe, J.Atmos.Oceanic Technol., 31, 2567-2567-2590, https://doi.org/10.1175/JTECH-D-13-00239.1, 2014.

Knollenberg, R. G.: Clouds their Formation, Optical Properties, and Effects, Anonymous Techniques for Probing Cloud Microstructure, Elsevier Inc, 15-91 pp. 1981.

Korolev, A. V. and I. P. Mazin: Zones of Increased and Decreased Droplet Concentration in Stratiform Clouds, J.Appl.Meteor., 32, 760-760-773, https://doi.org/ZOIADD>2.0.CO;2, 1993.

Korolev, A. V.: The Influence of Supersaturation Fluctuations on Droplet Size Spectra Formation, J.Atmos.Sci., 52, 3620-3620-3634, https://doi.org/TIOSFO>2.0.CO;2, 1995.

Korolev, A. V. and G. A. Isaac: Drop Growth Due to High Supersaturation Caused by Isobaric Mixing, J.Atmos.Sci., 57, 1675-1675-1685, https://doi.org/DGDTHS>2.0.CO;2, 2000.

Lamb, D. and J. Verlinde: Physics and Chemistry of Clouds. Cambridge University Press, 384-392 pp. 2011.

Lance, S., C. A. Brock, D. Rogers, and J. A. Gordon: Water droplet calibration of the Cloud Droplet Probe (CDP) and in-flight performance in liquid, ice and mixed-phase clouds during ARCPAC, Atmospheric Measurement Techniques, 3, 1683-1683-1706, https://doi.org/10.5194/amt-3-1683-2010, 2010.

Lawson, R. P., D. O'Connor, P. Zmarzly, K. Weaver, B. Baker, Q. Mo, and H. Jonsson: The 2D-S (Stereo) Probe: Design and Preliminary Tests of a New Airborne, High-Speed, High-Resolution Particle Imaging Probe, J.Atmos.Oceanic Technol., 23, 1462-1462-1477, https://doi.org/10.1175/JTECH1927.1, 2006.

Lawson, R. P., B. A. Baker, C. G. Schmitt, and T. L. Jensen: An overview of microphysical properties of Arctic clouds observed in May and July 1998 during FIRE ACE, J.Geophys.Res., 106, 14989-14989-15014, https://doi.org/10.1029/2000JD900789, 2001.

Marwitz, J., M. Politovich, B. Bernstein, F. Ralph, P. Neiman, R. Ashenden, and J. Bresch: Meteorological Conditions Associated with the ATR72 Aircraft Accident near Roselawn, Indiana, on 31 October 1994, Bull.Amer.Meteor.Soc., 78, 41-41-52, https://doi.org/MCAWTA>2.0.CO;2, 1997.

Pobanz, B. M., J. D. Marwitz, and M. K. Politovich: Conditions Associated with Large-Drop Regions, J.Appl.Meteor., 33, 1366-1366-1372, https://doi.org/CAWLDR>2.0.CO;2, 1994.

Politovich, M. K. and W. A. Cooper: Variability of the Supersaturation in Cumulus Clouds, J.Atmos.Sci., 45, 1651-1651-1664, https://doi.org/VOTSIC>2.0.CO;2, 1988.

Rasmussen, R. M., B. C. Bernstein, M. Murakami, G. Stossmeister, J. Reisner, and B. Stankov: The 1990 Valentine's Day Arctic Outbreak. Part I: Mesoscale and Microscale Structure and Evolution of a Colorado Front Range Shallow Upslope Cloud, J.Appl.Meteor., 34, 1481-1481-1511, https://doi.org/10.1175/1520-0450-34.7.1481, 1995.

Rasmussen, R. M., I. Geresdi, G. Thompson, K. Manning, and E. Karplus: Freezing Drizzle Formation in Stably Stratified Layer Clouds: The Role of Radiative Cooling of Cloud Droplets, Cloud Condensation Nuclei, and Ice Initiation, J.Atmos.Sci., 59, 837-837-860, https://doi.org/FDFISS>2.0.CO;2, 2002.

Rasmussen, R., M. Politovich, W. Sand, G. Stossmeister, B. Bernstein, K. Elmore, J. Marwitz, J. McGinley, J. Smart, E. Westwater, B. B. Stankov, R. Pielke, S. Rutledge, D. Wesley, N. Powell, and D. Burrows: Winter Icing and Storms Project (WISP), Bull.Amer.Meteor.Soc., 73, 951-951-974, https://doi.org/WIASP>2.0.CO;2, 1992.

Rauber, R. M.: Microphysical Structure and Evolution of a Central Sierra Nevada Orographic Cloud System, J.Appl.Meteor., 31, 3-3-24, https://doi.org/MSAEOA>2.0.CO;2, 1992.

Rauber, R. M. and L. O. Grant: The Characteristics and Distribution of Cloud Water over the Mountains of Northern Colorado during Wintertime Storms. Part II: Spatial Distribution and Microphysical Characteristics, J.Climate Appl.Meteor., 25, 489-489-504, https://doi.org/TCADOC>2.0.CO;2, 1986.

Rauber, R. M., L. S. Olthoff, M. K. Ramamurthy, and K. E. Kunkel: The Relative Importance of Warm Rain and Melting Processes in Freezing Precipitation Events, J.Appl.Meteor., 39, 1185-1185-1195, https://doi.org/TRIOWR>2.0.CO;2, 2000.

Rogers, R. R. and M. K. Yau: A Short Course in Cloud Physics. 3 ed. ed., International Series in Natural Philosophy, Butterworth Heinemann, US,121-130 pp. 1989.

Rosenfeld, D., R. Chemke, P. DeMott, R. C. Sullivan, R. Rasmussen, F. McDonough, J. Comstock, B. Schmid, J. Tomlinson, H. Jonsson, K. Suski, A. Cazorla, and K. Prather: The common occurrence of highly supercooled drizzle and rain near the coastal regions of the western United States, Journal of Geophysical Research: Atmospheres, 118, 9819-9819-9833, https://doi.org/10.1002/jgrd.50529, 2013.

Saleeby, S. M., W. R. Cotton, and J. D. Fuller: The Cumulative Impact of Cloud Droplet Nucleating Aerosols on Orographic Snowfall in Colorado, J.Appl.Meteor.Climatol., 50, 604-604-625, https://doi.org/10.1175/2010JAMC2594.1, 2011.

Tessendorf, S. A., J. R. French, K. Friedrich, B. Geerts, R. M. Rauber, R. M. Rasmussen, L. Xue, K. Ikeda, D. R. Blestrud, M. L. Kunkel, S. Parkinson, J. R. Snider, J. Aikins, S. Faber, A. Majewski, C. Grasmick, P. T. Bergmaier, A. Janiszeski, A. Springer, C. Weeks, D. J. Serke, and R. Bruintjes: A transformational approach to winter orographic weather modification research: The SNOWIE Project, Bull.Amer.Meteor.Soc., https://doi.org/10.1175/BAMS-D-17-0152.1, 2018.

Vali, G., R. D. Kelly, J. French, S. Haimov, D. Leon, R. E. McIntosh, and A. Pazmany: Finescale Structure and Microphysics of Coastal Stratus, J.Atmos.Sci., 55, 3540-3540-3564, https://doi.org/FSAMOC>2.0.CO;2, 1998.

Wang, J. and B. Geerts: Identifying drizzle within marine stratus with W-band radar reflectivity, Atmos.Res., 69, 1-1-27, https://doi.org/10.1016/j.atmosres.2003.08.001, 2003.

Wang, Z., J. French, G. Vali, P. Wechsler, S. Haimov, A. Rodi, M. Deng, D. Leon, J. Snider, L. Peng, and A. L. Pazmany: Single Aircraft Integration of Remote Sensing and In Situ Sampling for the Study of Cloud Microphysics and Dynamics, Bull.Amer.Meteor.Soc., 93, 653-653-668, https://doi.org/10.1175/BAMS-D-11-00044.1, 2012.

Wood, R., K. O, C. S. Bretherton, J. Mohrmann, B. A. Albrecht, P. Zuidema, V. Ghate, C. Schwartz, E. Eloranta, S. Glienke, R. A. Shaw, J. Fugal, and P. Minnis: Ultraclean Layers and Optically Thin Clouds in the Stratocumulus-to-Cumulus Transition. Part I: Observations, J.Atmos.Sci., 75, 1631-1631-1652, https://doi.org/10.1175/JAS-D-17-0213.1, 2018.

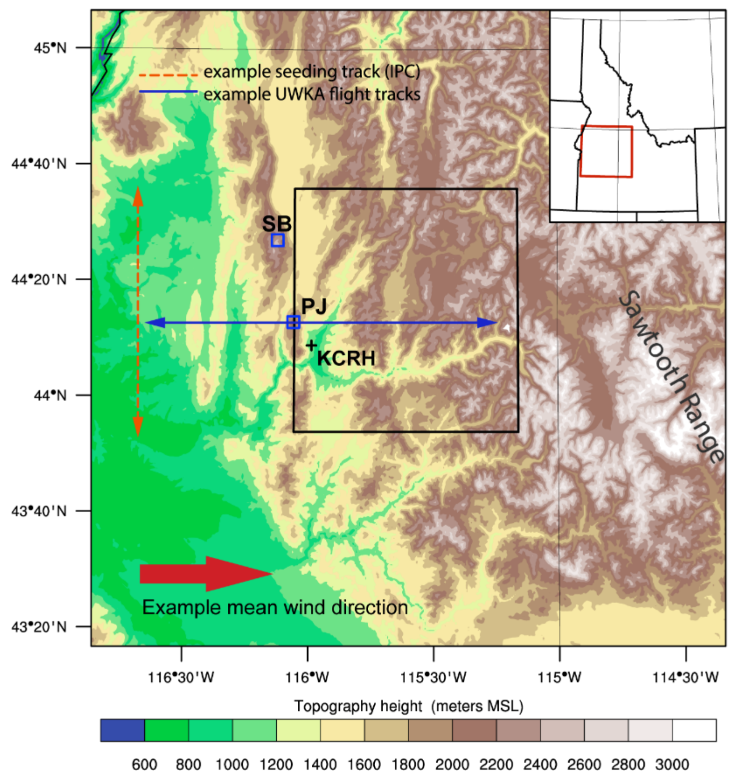

Figure 1: SNOWIE experimental setup showing a plan view schematic for an example case of westerly winds. Blue squares (□) correspond to the Snowbank (SB) and Packer John (PJ) ground sites, the plus sign (+) indicates the Crouch (KCRH) sounding launch site. The rendered topography domain is the same as in orange inset in the upper right hand corner of the figure. The black bounding box indicates the target seeding domain.

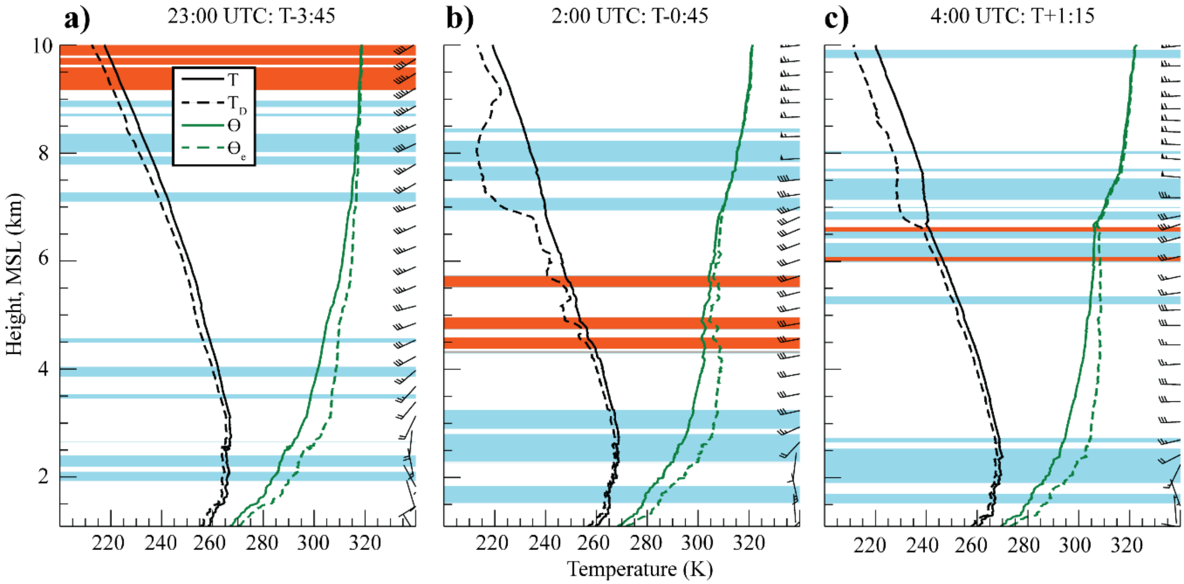

Figure 2: Thermodynamic and dynamic profiles from radiosondes launched at Crouch, ID (KCRH; Fig. 1). Shaded levels correspond to relaxed critical values of the bulk Richardson number, $Ri_{bulk} < 0.5$, after 10 pt (~50 m) vertical smoothing of the field. Orange shading indicates negative bulk Richardson values—corresponding to static instability—and blue corresponds to purely dynamic instability, $0 < Ri_{bulk} < 0.5$. Relative times (T +/-) reference the 2:45 UTC leg 1 start time.

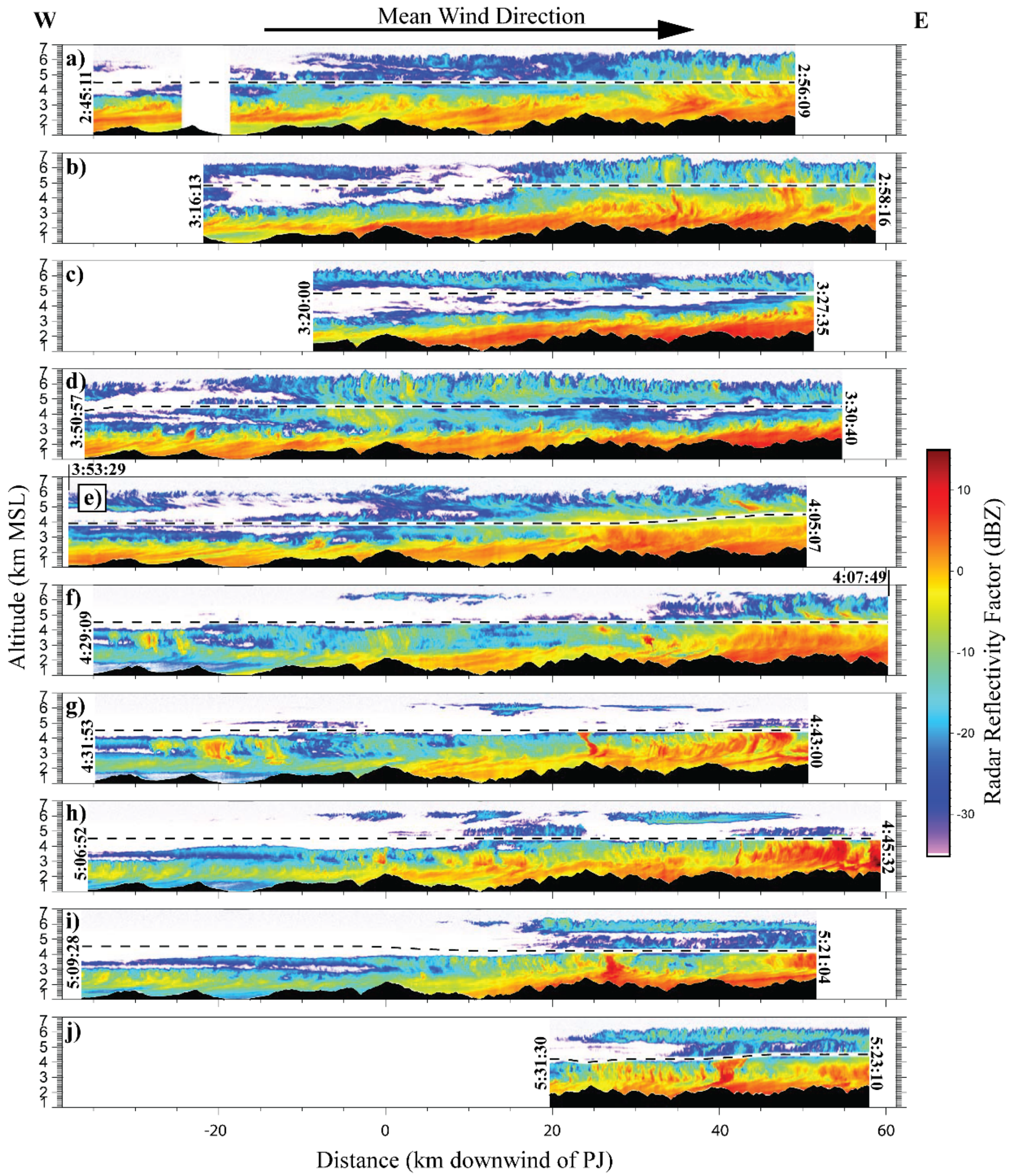

Figure 3: Terrain-Referenced W-band Radar Reflectivity cross sections for all 10 flight legs. All distances are relative to Packer John Mountain, with positive (negative) values downwind (upwind). Leg start and end times are in UTC, with (a) through (j) corresponding to legs 1 through 10, respectively.

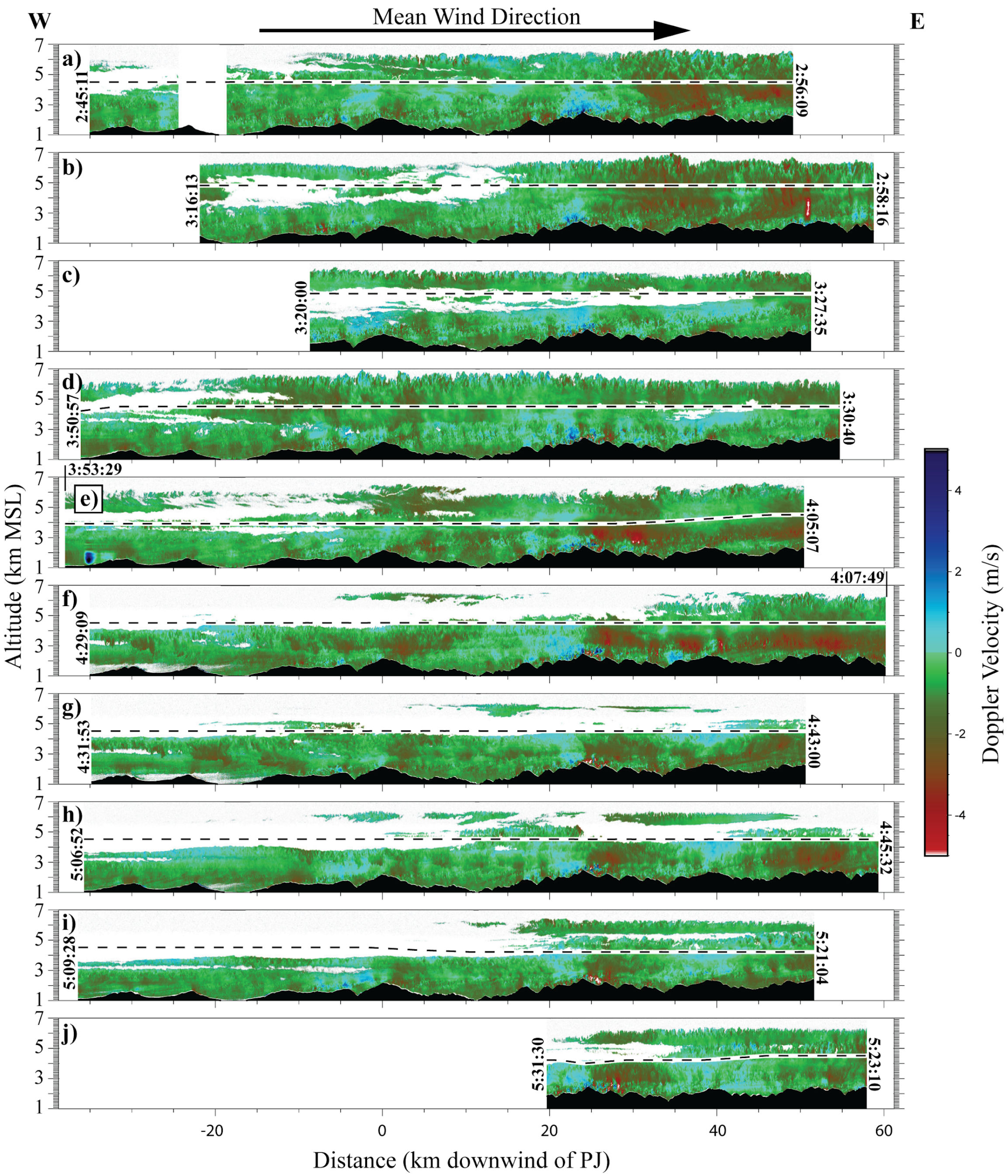

Figure 4: Terrain-Referenced W-Band Doppler Velocity Spatiotemporal cross sections for all 10 flight legs. All distances are relative to Packer John Mountain, with positive (negative) values downwind (upwind). Positive values of Doppler Velocity indicate upward motion. Leg start and end times are in UTC, with (a) through (j) corresponding to legs 1 through 10, respectively.

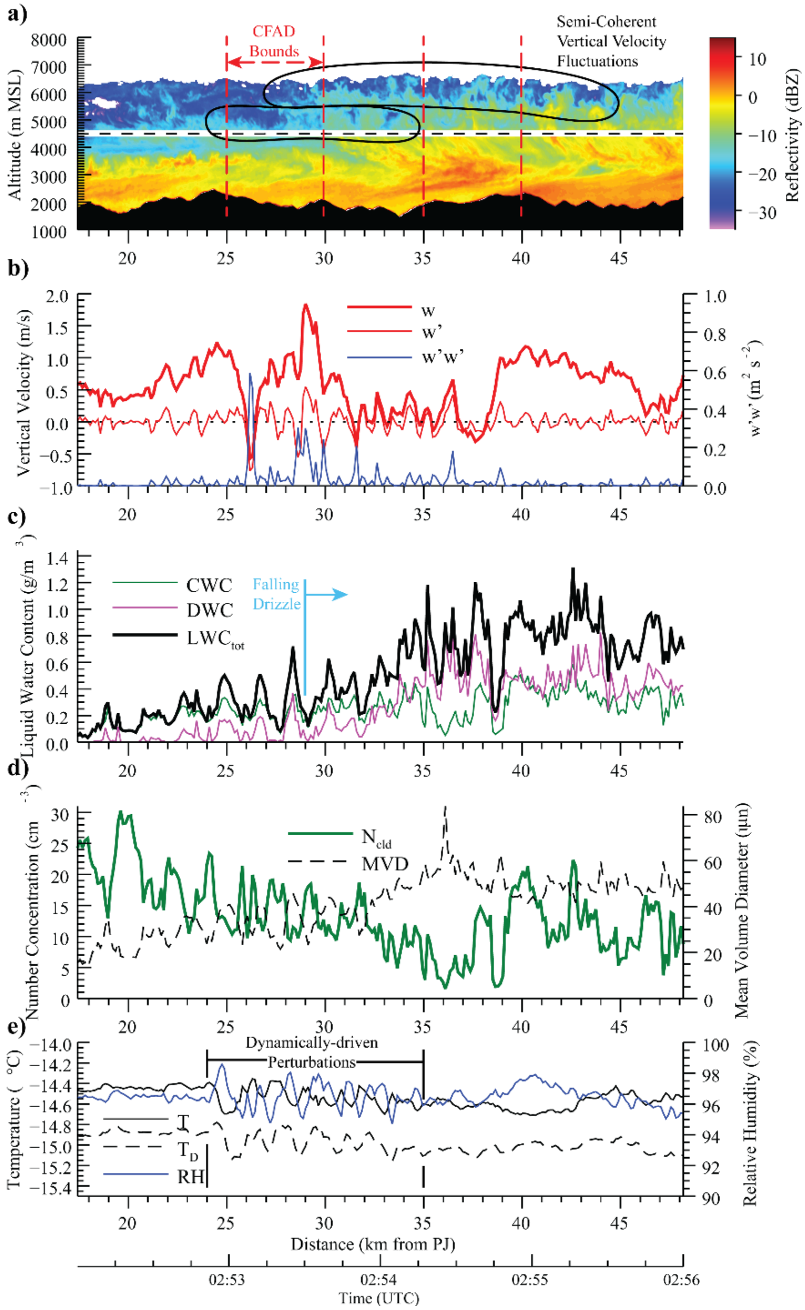

Figure 5: Detailed radar and in situ measurements for the drizzling portion of leg 1. Spatiotemporal vertical cross-sections of radar reflectivity are shown in (a). Graphs (b) through (e) are derived from flight-level in situ measurements and show: (b) vertical air velocity [w], computed perturbation vertical velocity [w'], and the variance of the perturbation vertical velocity [w'w'], (c) liquid water content derived from cloud droplets [CWC], drizzle drops [DWC], and both combined [LWC_{tot}], (d) cloud droplet number concentration [N_{cld}] and DSD mean-volume diameter [MVD] for all hydrometeors with D < 1.2 mm, and (e) temperature [T], dewpoint [T_D], and relative humidity [RH]. The CFAD bounds shown in (a) correspond to the columns for Fig. 8a-c. Perturbation vertical velocities in (b) were calculated by subtracting a boxcar-smoothed (over 10 s or roughly 1 km) vertical velocity field from the measured vertical velocity and represent the sub-kilometer vertical velocity perturbations.

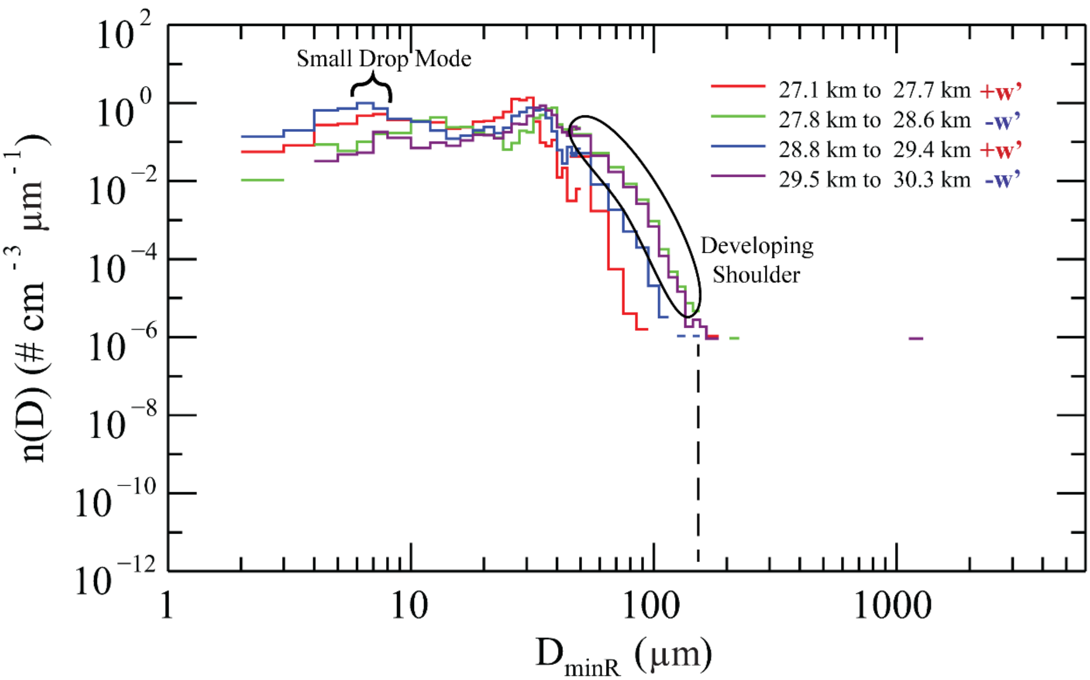

	Location	LWC_{CDP}	LWC_{comb}	N_{CDP}	MVD_{CDP}	MVD_{comb}
	km	*g m^{-3}*	*g m^{-3}*	*cm^{-3}*	*µm*	*µm*
+w’	27.1 - 27.7	0.155	0.182	16.988	25.950	27.238
-w’	27.8 - 28.6	0.251	0.452	12.242	33.955	39.599
+w’	28.8 - 29.4	0.177	0.217	15.528	27.897	29.676
-w’	29.5 - 30.3	0.267	0.438	12.127	34.786	39.499

Figure 6: Bin-width normalized averaged size distributions for representative perturbation up-/down-drafts within the flight-level sampled SCVVF train from leg 1. Table (b) contains calculated distribution parameters for the curves shown in (a). The corresponding location downwind of Packer John is given in the top right legend.

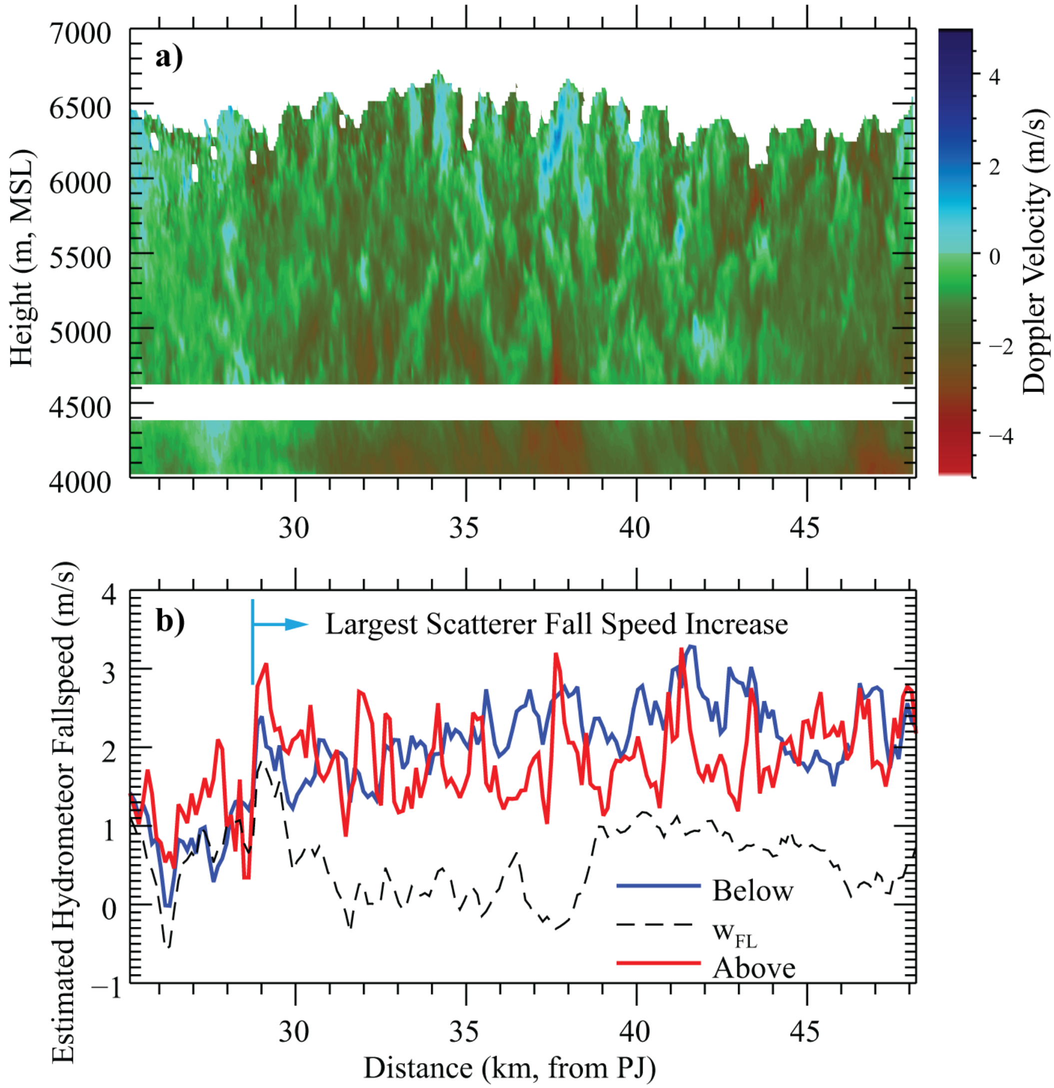

Figure 7: Doppler velocity and estimated hydrometeor terminal fall speed for a portion of Leg 1. Vertical cross section of Doppler velocity (a) and reflectivity-weighted hydrometeor population terminal fall speed (b)—estimated by flight level gust probe vertical velocity (black dashed) minus averaged Doppler velocity of the 3 nearest useable radar gates above (red) and below (blue) flight level.

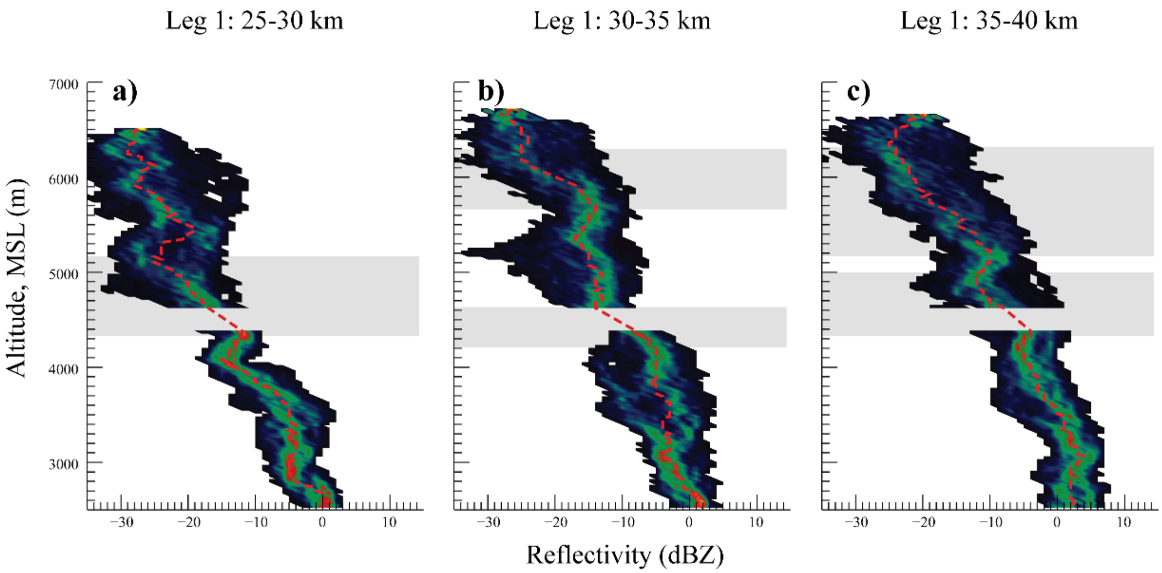

Figure 8: CFAD of radar reflectivity for three, 5 km-wide columns from leg 1, with relative location in km downwind of PJ indicated at the top of each panel. The dashed red line is the median reflectivity for a vertical level and frequency is normalized for each vertical level (same colors at top as any other level). Shading indicates the primary inferred growth regions within the elevated cellular layer.

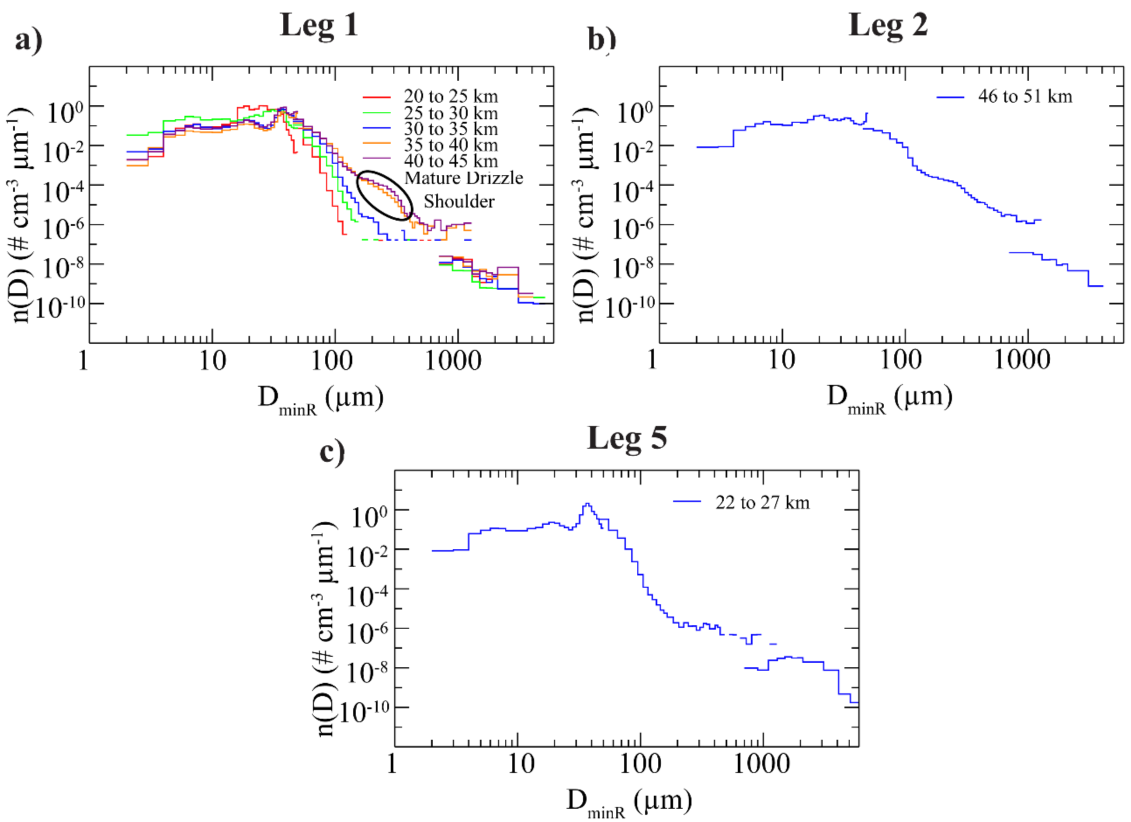

Figure 9: Averaged size distributions for legs 1, 2, and 5 (a, b, and c respectively) from the CDP, 2DS, and 2DP cloud and precipitation probes. Each of the blue composite size spectra correspond to the averaged size distributions at flight level during the CFADs in Fig. 12.

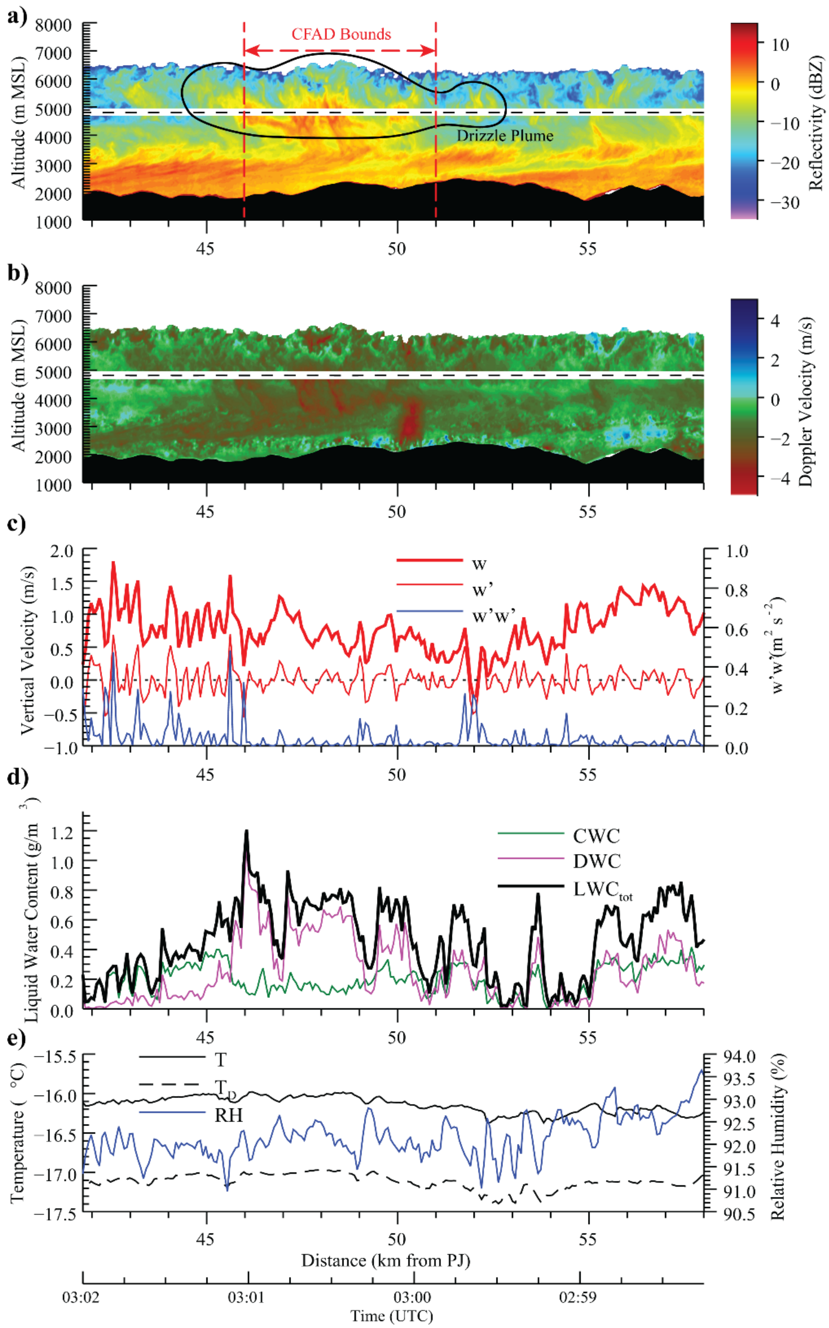

Figure 10: Detailed radar and in situ measurements for the drizzling portion of leg 2. Spatiotemporal vertical cross-sections of radar reflectivity are shown in (a) and vertical Doppler velocity are shown in (b). Graphs (c) through (e) are derived from flight-level in situ measurements and show: (c) vertical air velocity [w], computed perturbation vertical velocity [w'], and the variance of the perturbation vertical velocity [w'w'], (d) liquid water content derived from cloud droplets [CWC], drizzle drops [DWC], and both combined [LWC_{tot}], and (e) temperature [T], dewpoint [T_D], and relative humidity [RH]. The CFAD bounds shown in (a) correspond to the row from Fig. 12d-f. Perturbation vertical velocities in (c) were calculated as described in Fig. 5.

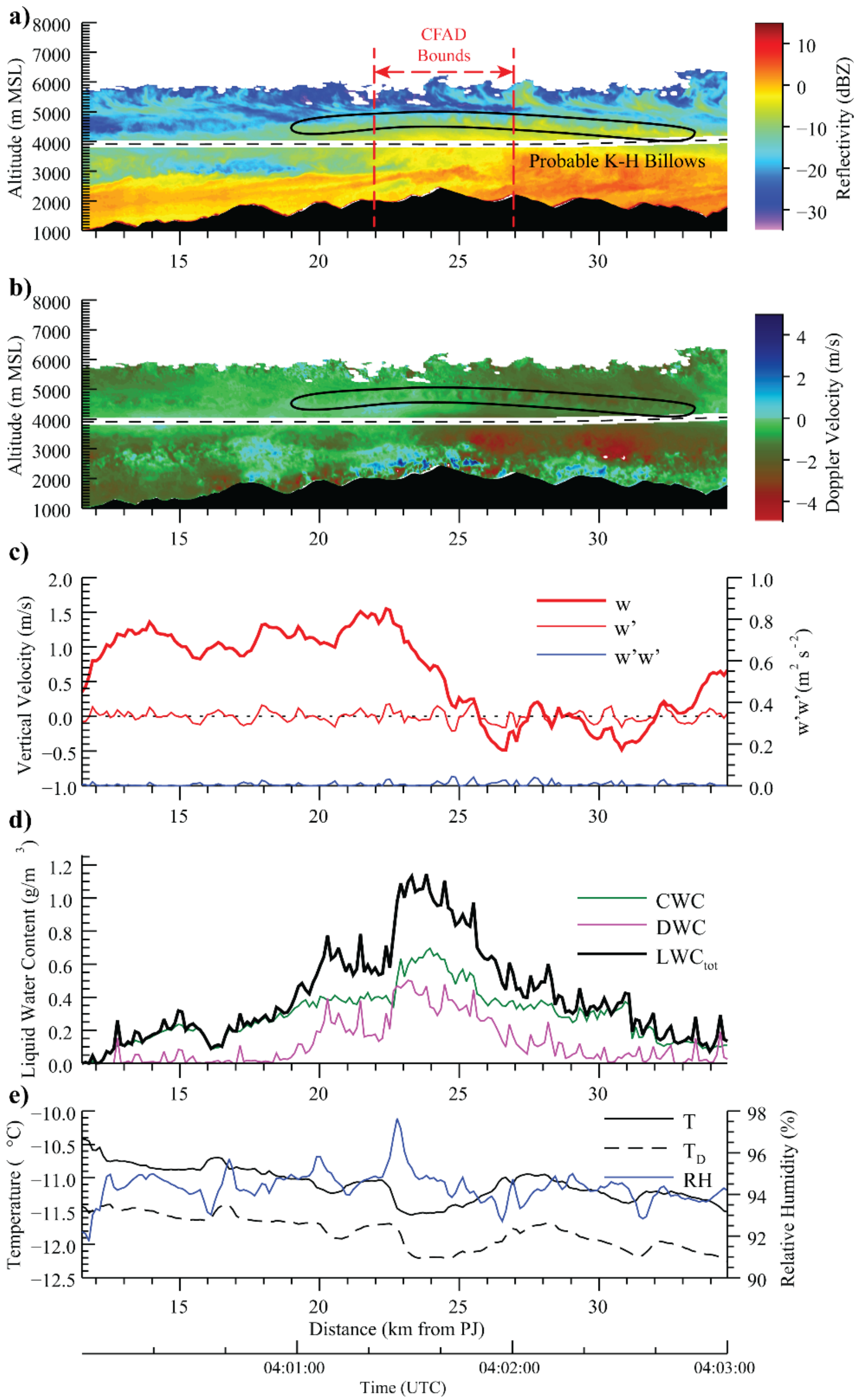

Figure 11: As in Figure 10 except for the drizzling portion of Leg 5. The CFAD bounds correspond to the row from Fig. 12g-i.

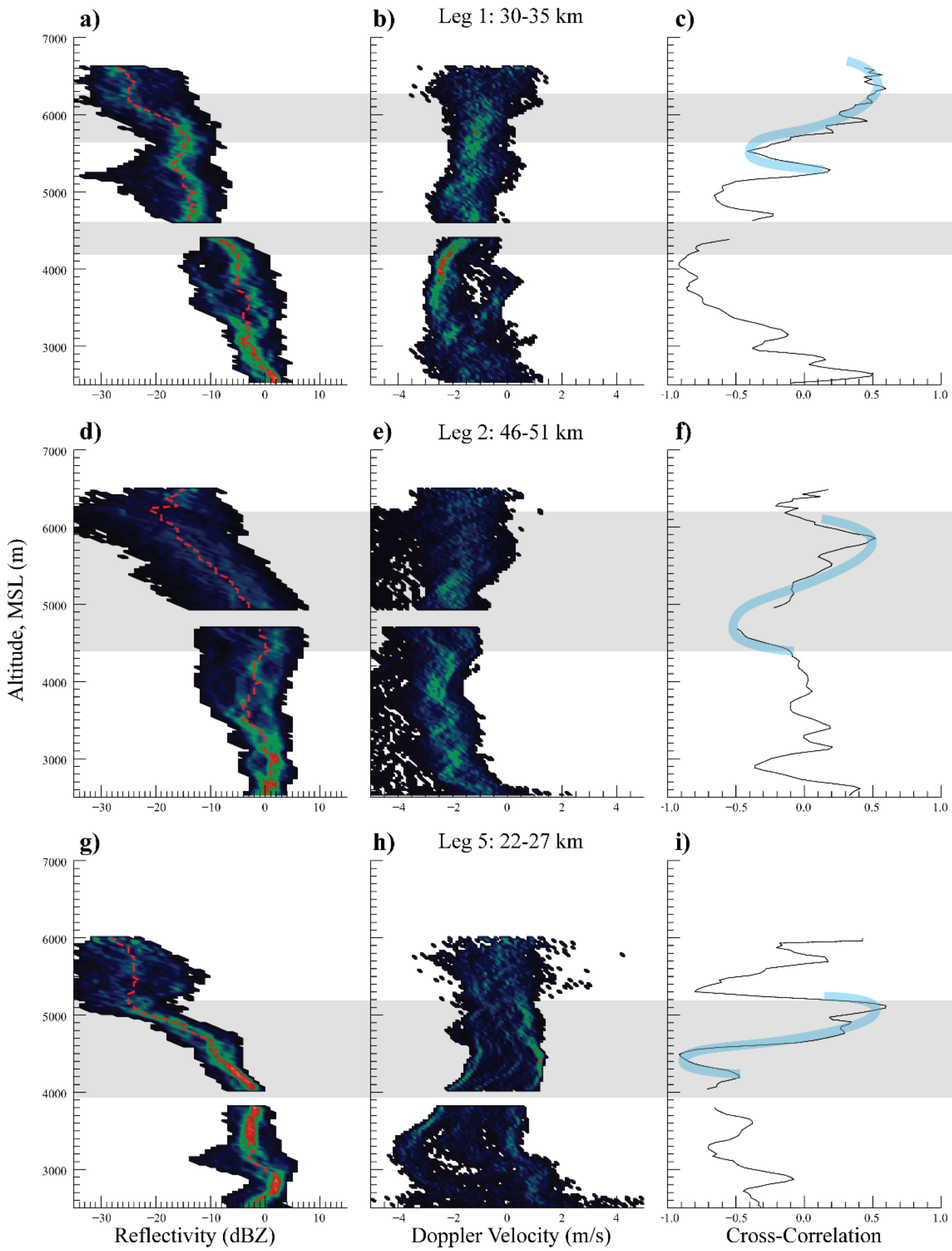

Figure 12: CFADs of reflectivity, Doppler velocity, and their 0-lag cross-correlation for the legs 1, 2, and 5 (rows 1-3, respectively, with relative distances downwind of PJ indicated at the top of each row). The dashed red line (left column) is median reflectivity for a vertical level and frequency is normalized for each vertical level (same colors at top as any other level). Vertical profiles of 0-lag cross correlation between reflectivity and Doppler velocity is shown in the right-most panel with reverse-S correlation patterns highlighted in light blue. Shading indicates the primary inferred growth regions within the elevated cellular layer.

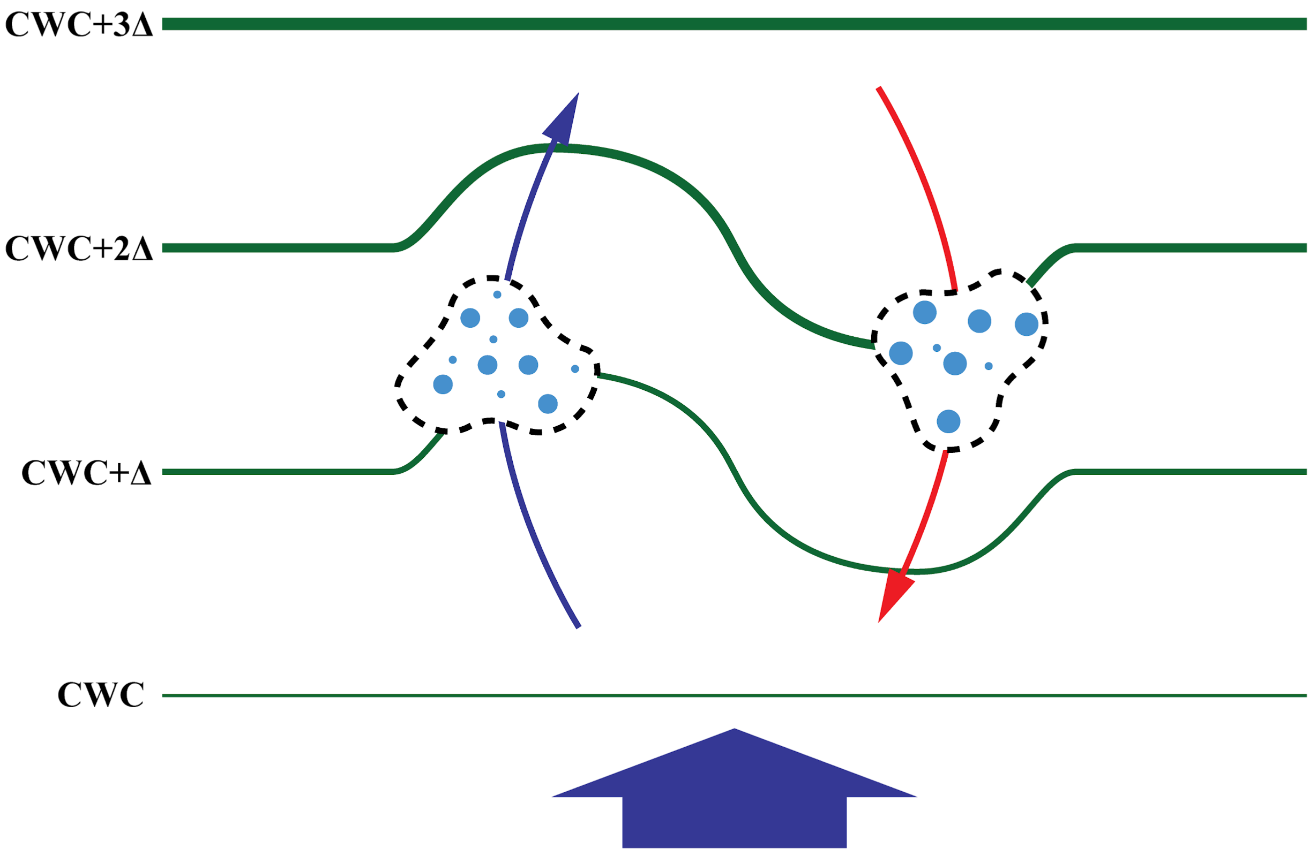

Figure 13: Simplified schematic of spatial responses to the perturbation updraft (blue) and downdraft (red) pattern superimposed on broader orographic lift (broad blue arrow bottom). The colored trajectories indicate the approximate path of parcels passing through the kinematic pattern following the schema of Houze and Medina (2005). Lines of constant cloud water content (green) indicating the expected deformations due to condensational kinetic effects, with line weight corresponding to relative condensate mass. Cloud parcels circulate within the vertical velocity perturbation pattern and more and smaller drops are located in perturbation updrafts than downdrafts. CWC contours appear flat and unperturbed above and below the vertical velocity fluctuation pattern as they are determined by the adiabatic ascent in the broader uplift pattern.

Probe	CDP	2DS	2DP
Measured Sizes	2 - 50 um	5 - 1285 um	0.4 - 16 mm
Sizing Technology	Forward Scattering	Optical Array	Optical Array
Temporal Resolution	5 Hz	1 Hz	1 Hz
Approximate Spatial Resolution	20 m	100 m	100 m

Table 1: Cloud Microphysics Probe Sizing and Technology

Leg	1	2	5
Altitude (m)	4500	4800	3900-4200
Temperature (°C)	-14.5	-16	-11
Gust Probe Vertical Velocity ($m\ s^{-1}$)	-0.5 to 2	-0.2 to 1.7	-0.5 to 1.5
Flight Level Perturbation Vertical Velocity Magnitude ($m\ s^{-1}$)	< 0.5	< 0.7	< 0.2
Cloud Water Content ($g\ m^{-3}$)	< 0.6	< 0.4	< 0.6
DWC in Plumes ($g\ m^{-3}$)	0.2 to 0.8	0.1 to 1.0	0.1 to 0.4
Cloud Droplet Number Concentration (cm^{-3})	2 to 30	3 to 30	8 to 35
Mean Volume Diameter (μm)	< 80	< 70	< 45
99^{th} Percentile Number Concentration of Precipitation-Sized Ice (L^{-1})	0.1	0.1	0.3

Table 2: Flight Level Cloud Characterization Information Between Legs 1, 2, and 5